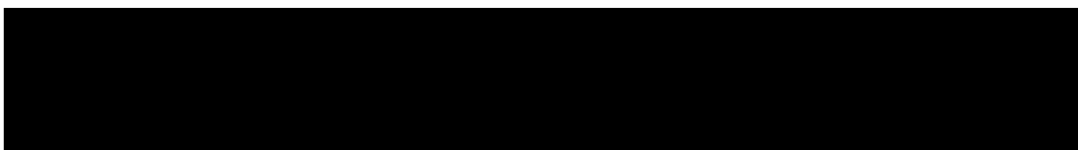# Master thesis

Study program energy technology

Techno-economic analysis of a co-electrolysis process with the integration of concentrated solar energy

Hannah Ninette Lindermeir

Abstract

The present work analyzes a co-electrolysis process to produce syngas. The thermal energy required for this high temperature electrolysis is provided by concentrated solar energy. To determine the thermal and electrical energy requirements, the process is simulated in aspen plus. In order to find a suitable electrolyzer model for the simulation in aspen, the simulations and experimental data of different publications are compared with each other and with the results of the own simulations. A model with an equilibrium reactor, a stoichiometric reactor, a separator and another equilibrium reactor is suitable as an electrolyzer model. All components operate at the same temperature. In this way, deviations between simulation results and experimental data of far less than 5 % are achieved. The specific thermal energy demand to produce one kmol of syngas is 46.9 kWh, the specific electric energy demand is 300.7 kWh per kmol of syngas. The simulation results are used as input for a transient analysis to determine the annual electrical and thermal energy requirements and to estimate the annual syngas production rate. Using a parameter study, the size of the heliostat field, the nominal load of the electrolyzer and the storage capacity are optimized. Approximately 89,700 tons of syngas can be produced per year. A brief economic analysis calculates the levelized cost of syngas to be 822 €/kg syngas.

Table of contents

Table of contents

List of figures

List of tables

List of tables

List of abbreviations

List of abbreviations

C .... *charge*
chem .... *chemical*
CSP .... *concentrated solar power*
D ....*discharge*
eva.. *evaporate*
HT .... *high temperature*
HTE .... *high temperature electrolyzer*
HX ....*heat exchanger*
LCOS .... *levelized cost of syngas*
LT.. *low temperature*
PEM .... *proton exchange membrane*
RU..*reactant utilization*
RWGS ....*reverse water gas shift*
SB ....*standby*
SOC... *state of charge*
sup... *superheated*
thermal energy storage ....*TES*

List of symbols

symbol	Symbol description	unit
A	Area	m²
A	Annual cost	€/year
C	Investment costs	€
E	Energy	Wh
F	Faraday constant	C/mol
f	Relative agreement/deviation	-
f	Fraction	-
G	Gibbs energy	J
H	Enthalpy	J
h	Specific enthalpy	J/kg
i	Interest rate	%
M	Molar mass	g/mol
m	Mass	kg
$\dot{m}$	Mass flow	kg/sec
mr	Molar ratio	-
n	Lifetime	a
$\dot{n}$	Mole flow	mol/sec
P	Power	W
p	Specific electrical energy	Wh/mol
q	Specific thermal energy	Wh/mol
Q	Thermal energy	Wh
$\dot{Q}$	Thermal power	W
S	Entropy	J/K
T	Temperature	K
t	Time	hr
U	Cell voltage	V
$\dot{V}_N$	Norm volume flow	Nm³/sec
x	Molar fraction	-
x	Factor	-
η	Efficiency	-
ϑ	Temperature	°C
ρ	Density	kg/m³
φ_N	Norm volume fraction	-

1   Introduction

Decarbonization is an essential building block on the path to a CO_2-neutral society. Electrification of all CO_2 emitting sectors is difficult to achieve. The use of hydrogen or synthetically produced hydrocarbons is necessary. The latter can be used as a raw material for various chemical industries or as a fuel for aviation and shipping. Of particular interest is the production of syngas, a mixture of carbon monoxide and hydrogen from which many other hydrocarbon chains can be produced. It can be used in a variety of ways, for example in the production of chemicals, pharmaceuticals or biofuels (Langie et al., 2022). Its use as a raw material for alternative fuels seems particularly interesting because the existing infrastructure and engine technology can remain unchanged (Fu et al., 2010). In particular, fuel produced from syngas has potential for heavy-duty vehicles, aviation and shipping, as these sectors can only be electrified to a limited extent (Ausfelder & Wagemann, 2020).

To date, syngas has been produced mainly by coal gasification and steam reforming of natural gas (Bachmann et al., 2023; Hawkes, 2007; Stoots et al., 2009). In recent years, other promising production options have been developed. For example, syngas can be produced from steel plant off-gas capture (mill gas). Typically used for internal heat and power recovery in steel production, mill gas can also be captured and used as a feedstock for chemicals. Another option are bio-based technologies. These use anaerobic digestion and gasification (Bachmann et al., 2023). A third option is CO_2-based syngas production using carbon capture and utilization. The CO_2 is used, for example, as a feedstock for the reverse water gas shift reaction, the Sabatier process, the reaction swing absorption or is reduced electrochemically (Bachmann et al., 2023; Langie et al., 2022). When used for the electrochemical reduction it can be separated in the CO_2-electrolysis or together with hydrogen in the high temperature co-electrolysis. The production of syngas by high-temperature electrolysis is promising because it allows an increase in efficiency compared to the production route using low- temperature electrolysis and reverse water gas shift reactions (Hawkes, 2007). In high-temperature electrolysis, part of the energy required can be provided by heat. The integration of concentrated solar power is well suited for providing the thermal energy to reach required temperatures above 800 °C.

Advantages of co-electrolysis compared to separate electrolysis of water and CO_2 are simplifying the system and rising the efficiency. Only one electrolyzer is needed and the reactor for the reverse water gas shift reaction can be eliminated (Graves et al., 2011; Herz et al., 2018). The likelihood of producing pure coal is reduced (Hawkes, 2007). The area specific resistance in CO_2 electrolysis is much higher than in steam electrolysis. In co-

Introduction

electrolysis it is mainly the steam that is reduced and the RWGS is mainly responsible for the carbon monoxide production. The area specific resistance changes only slightly in co-electrolysis compared to steam electrolysis (Fu et al., 2010; Stoots et al., 2009).
It can be said that co-electrolysis is a promising option for the efficient and sustainable production of syngas. Especially when part of the required energy is provided by solar energy. To ensure continuous operation, the use of thermal energy storage (TES) systems is a good option.

To date, there is little experimental data on co-electrolysis. Different approaches are used to model the co-electrolysis. Some models may not consider all relevant physical processes, which leads to different results. The limited availability of experimental data complicates the validation of simulation models. Without sufficient comparative data, it is difficult to verify the accuracy of the models.

The aim of this thesis is a techno-economic analysis of a solar high temperature co-electrolysis. As a basis, a model of a process is developed. Simulation studies in Aspen Plus are used to determine the required electrical and thermal energy demand. The process simulation is verified by a parameter study using literature data. Simulation studies in Python are used to determine the required electrical and thermal energy demand and to investigate the sensible integration of high and low temperature storage systems. Furthermore, the economic indicators for different process configurations are determined. An annual yield simulation will support the dimensioning of the system. For this purpose, an existing Python model for the steam electrolysis process will be adapted and used.

2   Basics

This chapter is composed by four main sections and briefly describes the basic terms used in this thesis. First, some basic conversions necessary for this work are presented. Then information about high temperature electrolysis and co-electrolysis is given. The last part of this chapter is dedicated to some information about concentrated solar energy.

2.1   Conversions

Some conversions that will be important later are listed here. Depending on what is given, the mole flow can be calculated using Formula (1) or (2).

$$\dot{n}_i = \frac{\dot{m}_i}{M_i} \tag{1}$$

$$\dot{n}_i = \frac{\dot{V}_{N,total} * \varphi_{N,i} * \rho_i}{M_i} \tag{2}$$

$\dot{V}_N$ is the norm volume flow and φ_N is the norm volume fraction. The molar fraction can be calculated with Formula (3), the volume/mass fraction with the same scheme using the volume/mass flows instead of the mole flows.

$$x_i = \frac{\dot{n}_i}{\dot{n}_{total}} \tag{3}$$

The mass flow is calculated using Formula (4).

$$\dot{m}_i = \frac{\varphi_i \cdot \dot{V}_N}{\rho_i} \tag{4}$$

2.2   High temperature electrolysis

A steam electrolyzer splits water into hydrogen and oxygen (see Formula (5)).

$$H_2O = H_2 + 0.5\ O_2 \tag{5}$$

This process has been established worldwide for more than 100 years. Alkaline and proton exchange membrane (PEM) electrolysis are already widely available. High temperature electrolysis is promising, but has a very small market share (Peters et al., 2022). However, due to the higher production costs, hydrogen is currently produced mainly by steam reforming of natural gas, partial oxidation of mineral oil or coal gasification (Schmidt, 2022; Töpler & Lehmann, 2017).

Basics

Thermal splitting of steam requires temperatures of several thousand degrees Celsius (Töpler & Lehmann, 2017). Another option is to spit water electrolytic.

$$\Delta H = \Delta G + \Delta S \cdot T \qquad (6)$$

The enthalpy of the reaction is made up of an entropy component and free Gibbs energy (see formula (6)). The free Gibbs energy is provided electrically and the entropy component thermally. At 25 °C, this requires a cell voltage of 1.23 V as long as the part for $T \cdot \Delta s$ is thermally provided (Schmidt, 2022).

This relationship is illustrated in Figure 1. As the temperature increases, the electrical energy requirement decreases and the thermal energy requirement increases. At 1000 °C, a cell voltage of 0.91 V is required compared to 1.23 V at 25 °C. This means that energy efficiency is improved at higher temperatures because less electrical energy is required to perform the same reaction (Schmidt, 2022). The Nernst equation describes this relationship between temperature and cell voltage, where temperature has a direct effect on the thermodynamic forces in the electrolysis. This is a major advantage of high-temperature electrolysis, as thermal energy is often cheaper as electrical energy (Fu et al., 2010).

Co-electrolysis is a high temperature electrolysis and is described in more detail below.
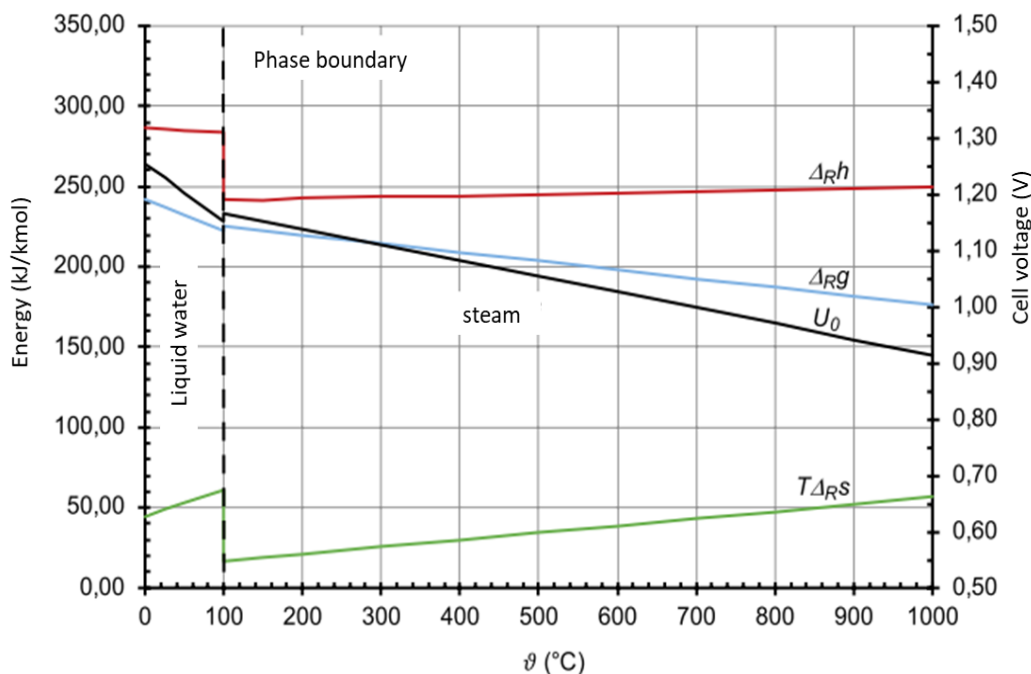
Figure 1 thermodynamics of the steam electrolysis. The right axes show the corresponding cell voltage of the energy needed. Based on (Schmidt, 2022)

Basics

2.3 Co-electrolysis

This section describes the thermodynamic reactions and the process operating conditions of the co-electrolysis process.

2.3.1 Thermodynamic reactions of the co-electrolysis process

During co-electrolysis, water and carbon dioxide are reduced to form hydrogen, carbon monoxide and oxygen. As seen in Figure 2, the reduction of water and carbon dioxide is taking place at the cathode (fuel electrode), the oxygen ions released in the process migrate through the electrolyte to the anode (air electrode), where they are oxidized to form oxygen molecules.
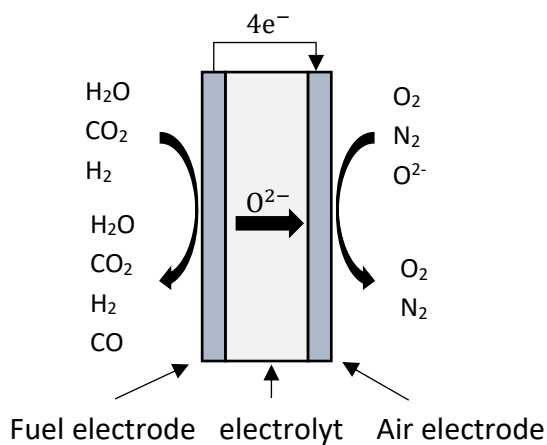
Figure 2 co-electrolysis. Based on (Roeder, 2023)

In addition to the endothermic reduction reactions (cf. Formula (7) and(8)), the reverse water gas shift (RWGS) reaction also takes place. In this equilibrium reaction (cf. Formula (9)), carbon dioxide and hydrogen react to form carbon monoxide and water (Dueñas et al., 2020).

$$H_2O = H_2 + 0.5\,O_2 \tag{7}$$

$$CO_2 = CO + 0.5\,O_2 \tag{8}$$

$$CO_2 + H_2 = CO + H_2O \tag{9}$$

If the cell voltages are too high, carbon may form (cf. Formula (10)). To avoid carbon formation, the electrolysis cell should be operated at low voltages (Redissi & Bouallou, 2013). The formation of carbon should be avoided because the solid carbon particles can contaminate the cell. This will result in a reduction in cell performance (Hawkes, 2007).

$$CO \rightarrow C + 0.5\,O_2 \tag{10}$$

Basics

Methane is formed from carbon monoxide and hydrogen at temperatures of 300 to 700 °C (see Formula (11)). This reaction is exothermic, but must be accelerated by a catalyst, usually nickel. If nickel is used as a catalyst, the operating temperature should be higher than 700 °C to avoid methane formation (Stoots et al., 2009).

$$CO + 3\,H_2 \leftrightarrow CH_4 + H_2O \qquad\qquad (11)$$

The relationship between temperature and cell voltage for co-electrolysis is shown in Figure 3. It can be seen that as the temperature increases, the electrical energy demand decreases and the thermal energy demand increases. Compared to operation at 25 °C, the cell voltage can be reduced by 0.14 V at 800 °C.
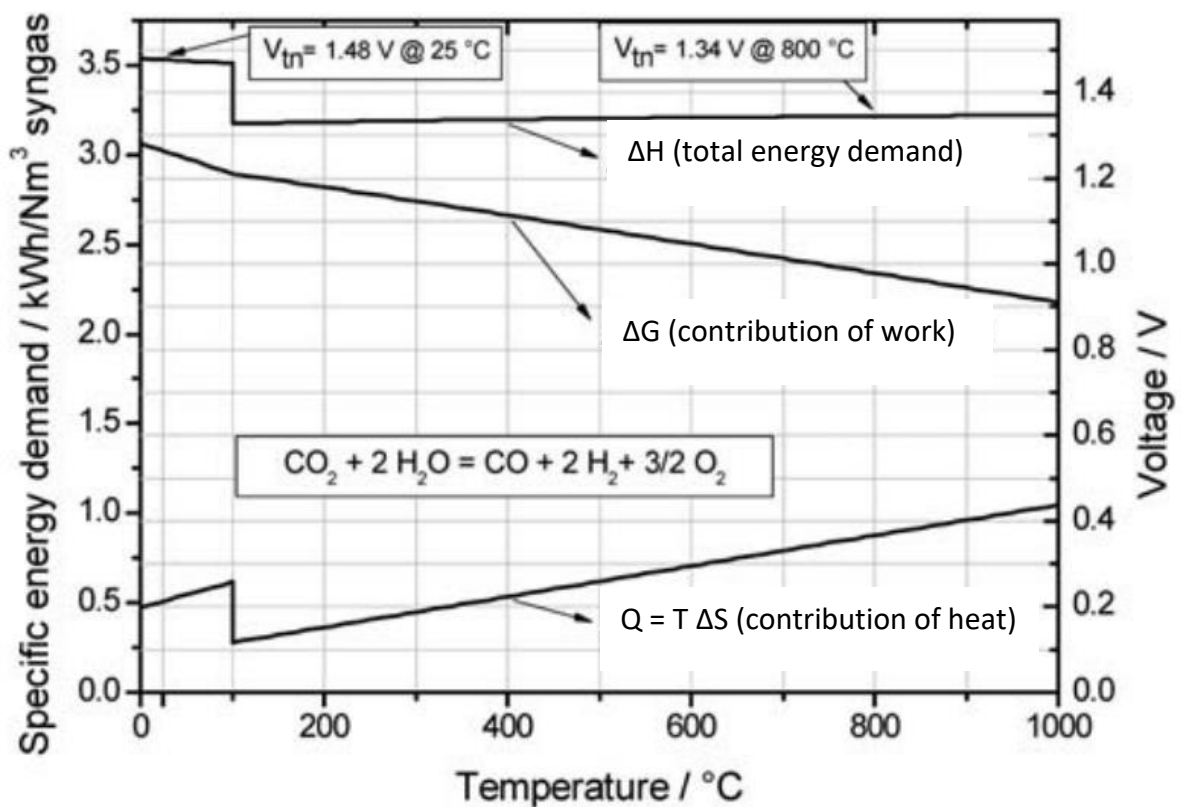
Figure 3 thermodynamics of the co electrolysis process. The right axes show the corresponding cell voltage of the energy needed. Based on (Fu et al., 2010).

2.3.2 Process operating conditions

The electrolyzer can be operated in three different ways depending on the operating voltage. Thermoneutral operation means that there is no need to add or remove heat. The enthalpy increase of the reactions is exactly balanced with the electrical energy input. If the

Basics

electrolyzer had optimal isolation, the inlet and outlet temperatures would be the same. If the electrolyzer operating voltage is below the thermoneutral voltage, the endothermic reactions predominate, the stack cools down and heat must be added. Above the thermoneutral voltage, ohmic losses dominate and heat must be removed (Fu et al., 2010; Petipas et al., 2013; Stoots et al., 2009). Thermoneutral operation is preferred because it minimizes local temperature gradients and associated mechanical stresses (Fu et al., 2010). To achieve isothermal operation, the electrolyzer is operated slightly above the thermoneutral voltage to counteract heat losses (Fu et al., 2010; Larsen & Sønderberg Petersen; Tomberg et al., 2023).

The thermoneutral voltage for co-electrolysis depends on the inlet composition, oxygen utilization and temperature. The thermoneutral voltage at 800 °C for steam and carbon dioxide is 1.29 V and 1.46 V (Stoots et al., 2009). As the inlet composition contains more water and hydrogen than CO and CO_2 the thermal neutral voltage for co-electrolysis is closer to the thermoneutral voltage for steam electrolysis. Typical voltages are between 1.32 V and 1.34 V (Dueñas et al., 2020; Hawkes, 2007; Stoots et al., 2009).

As shown in Figure 2, air flows through the air electrode. It is not necessary to flow air through the anode. If this is not done, pure oxygen can be produced as a by-product (Fu et al., 2010). However, there are significant technical problems associated with handling pure oxygen at high temperatures, which can negatively affect the performance of the cell. When the oxygen content is greater than 40%, the likelihood of nickel oxidation on the electrode increases (O'Brien et al., 2010; Peters et al., 2022).

2.4 Concentrated solar power

Concentrating solar power (CSP) technologies use lenses and mirrors, individually or in combination, to concentrate direct beam solar radiation and convert the energy into other forms, such as electricity, heat or fuels, through a variety of downstream systems.

Unlike photovoltaic, which also uses diffuse radiation, CSP systems can only use the direct component of solar radiation. For this reason, they are best suited to locations with low cloud cover and low smog or dust concentrations. This enables them to reach high temperatures most of the year. The main parameter affecting CSP production is therefore the Direct Normal Irradiance (DNI). The DNI represents the amount of radiation received per unit area on a surface perpendicular to the sun [kWh/m²] (Lovegrove, 2021).

Figure 4 shows how CSP is used in the co-electrolysis process.

Basics

HX 1: Evaporation; HX 2: Superheating Steam; HX 3: Superheating Air
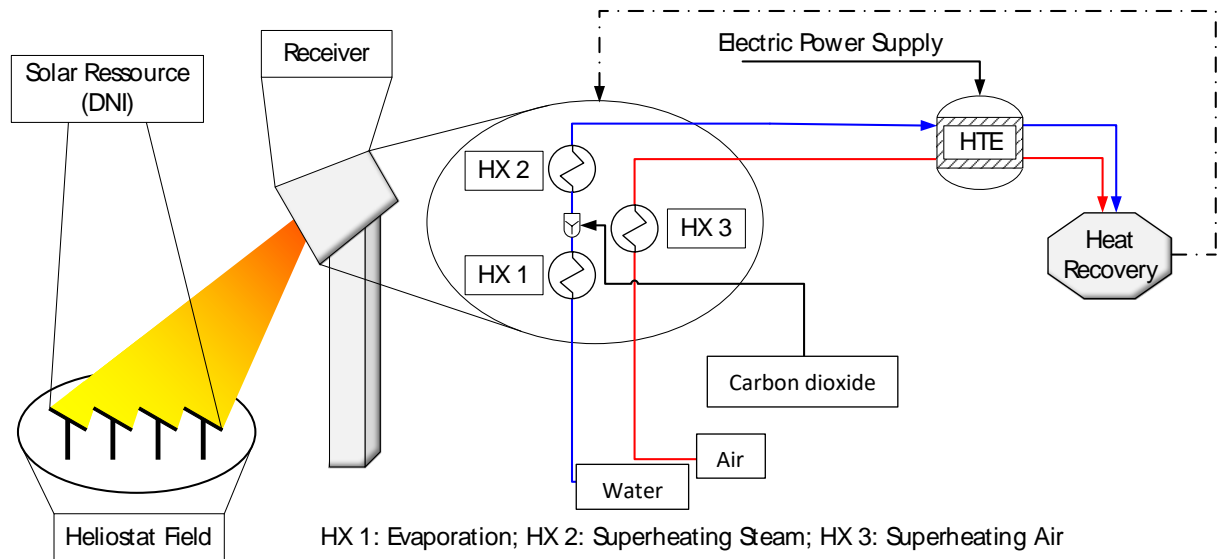
Figure 4 process overview co-electrolysis with heat recuperation and integration of concentrated solar energy. Based on (Roeder, 2023).

Solar radiation is concentrated using a field of heliostats. These heliostats track the sun and redirect the sunlight to a receiver. In the receiver, the concentrated solar energy heats various material streams. In particular, water is evaporated. The water vapor is then mixed with carbon dioxide. The combined water/carbon dioxide mixture is superheated. In addition to the water/carbon dioxide mixture, air is also superheated by the concentrated solar energy. The heated streams are directed to an electrolyzer. After electrolysis, the output streams still contain heat. To maximize energy efficiency, as much heat as possible is recovered from the output streams.

3   Process simulation

The objective is to integrate concentrated solar energy into a co-electrolysis process. To achieve this, the thermal energy requirement is necessary. The thermal energy depends on the electrolyzer. This chapter discusses the study of an electrolyzer model.

3.1   Method

To determine the energy requirements needed for co-electrolysis, the process is simulated in Aspen plus. A simplified overview of the process is shown in Figure 5.

The four material flows water, air, carbon dioxide and hydrogen are heated in different ways, mixed and fed to the electrolyzer. The thermal energy of the output streams of the electrolyzer is recovered through several heat exchangers (HX) (HX5 to HX8). This heat recovery will be discussed in more detail later. Another source of thermal energy is provided by heat exchangers 1 to 3. They receive their thermal energy from solar energy. HX4 heats up hydrogen. Hydrogen is highly volatile and tends to accumulate in steel voids. Therefore, hydrogen is added to the process as late as possible because the pipes require high quality and expensive alloys (Schmidt, 2022). Due to the complexity of the material, hydrogen is not preheated via a heat exchanger or solar energy, but electrical.
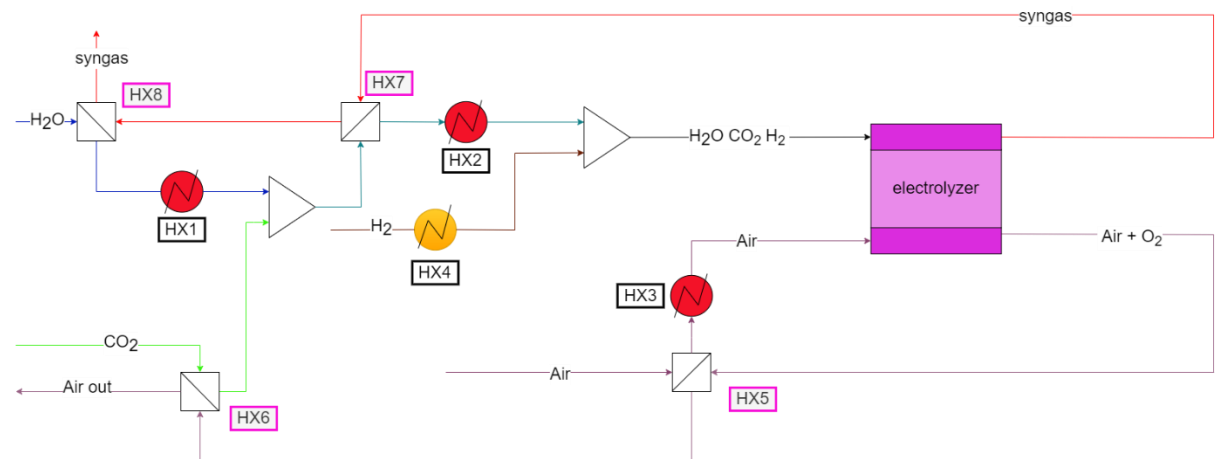
Figure 5 process overview co electrolysis

Aspen does not include a prebuilt model for the co-electrolysis. In order to simulate an electrolysis process, various individual blocks are assembled. In the past, different reactor configurations were used in literature.

In the next chapter a literature review is performed. It is examined how previous simulations have been carried out and what results they have yielded. Subsequently, with the help of

Process simulation

literature references, various models of the electrolyzer in Aspen are developed and adapted to the planned operating conditions.

3.1.1 Literature

Five publications were used as the basis for the review. They were published over a period of ten years. They have different objectives and input data. Therefore, they cover different possible operating conditions. Most papers have performed simulations. Redissi & Bouallou, 2013 and Khesa & Mulopo, 2021 both simulated the co-electrolysis with aspen plus. Tomberg et al., 2023 simulated with DLR's modelling and simulation framework TEMPEST. Dueñas et al., 2020 has experimental data. Tandl, 2023 simulated in AVL SOC simulation environment and has experimental data.

3.1.1.1 Literature input

The first step is to examine what is used as input in the five publications. Table 1 shows the reactant utilizations (RU) and temperatures used in the process, as well as the year of publication. The RU sets the input and output streams of the electrolyzer into relation and is needed as an input for the stoichiometric reactor for the simulation in Aspen.

Table 1 input data publications

input	(Tomberg et al., 2023)	(Dueñas et al., 2020)	(Khesa & Mulopo, 2021)	(Redissi & Bouallou, 2013)	(Tandl, 2023)
RU H_2O	0.7	0.2	0.526	0.98	0.73
RU CO_2	0.7	0.2	0.3932	0.05	0.73
RU syngas			0.438/0.483		
temperature in °C	830	860	700	800	825
year of publication	2022	2020	2020	2013	2023

The temperatures vary between 700 and 860 °C. Temperature affects reaction kinetics and energy requirements. The 700 °C in Khesa and Mulopos' publication is the most different from the others and is at the lower end of the desired operating conditions, as lower temperatures increase the likelihood of methane formation.

The RUs are very different. In the case of Khesa and Mulopo, four RUs are given in the paper. Two for syngas (0.438 and 0.483) and one each for water (0.526) and carbon dioxide (0.3932).

Process simulation

Redissi and Bouallou states conversion rates of $X_{H_2O} = 0.98$ for water and $X_{CO_2} = 0.05$ for carbon dioxide. RUs well above 90 % for steam is operationally impractical because localized cell steam starvation can occur. This can result in severe degradation and possibly faster cell life degradation (O'Brien et al., 2010). To find out which of the RUs are being used, the RUs for H_2O and CO_2 are calculated with the following formulas (Formula (12) and (13)).

$$RU_{H_2O} = \frac{\left|\dot{n}_{H_2,inlet} - \dot{n}_{H_2,outlet}\right|}{\dot{n}_{H_2O,inlet}} \tag{12}$$

$$RU_{CO_2} = \frac{\left|\dot{n}_{CO,inlet} - \dot{n}_{CO,outlet}\right|}{\dot{n}_{CO_2,inlet}} \tag{13}$$

For the calculation the inlet and outlet mole flows are needed. The inlet mole flows are both given. The outlet mole flows need to be calculated.

In the publication of Khesa and Mulopo, outlet molar fractions are given. The molar fraction of water however refers to a different molar flow than the other substances (CO_2, H_2O and CO). Mole flows of both streams are given, so the water mole flow can be calculated with Formula (14). Mole flows of H_2, CO and CO_2 can be calculated with Formula (15).

$$\dot{n}_{H_2O} = \dot{n}_{H_2O,O_2} * X_{H_2O} \tag{14}$$

$$\dot{n}_{H_2} = \dot{n}_{product} * X_{H_2} \tag{15}$$

In Redissi and Bouallou s paper only the outlet mass flows of hydrogen and carbon monoxide are given. Dividing these by the molar mass results in the molar flows (see Formula (16)).

$$\dot{n}_{i,outlet} = \frac{\dot{m}_i}{M_i} \tag{16}$$

Table 2 shows the calculated and reported RUs for Khesa and Mulopo and Redissi and Bouallou .

Table 2 calculated and published reactant utilizations

model	Khesa & Mulopo, 2021		Redissi & Bouallou, 2013	
	calculated	given	calculated	given
RU H_2O	0.4355	0.526	0.4630	0.98
RU CO_2	0.4458	0.3932	0.5773	0.05
RU syngas		0.438/0.483		

Process simulation

Other important input data are the inlet molar fractions shown in Figure 6. A table with the exact values can be found in the appendix A (see Table 18).
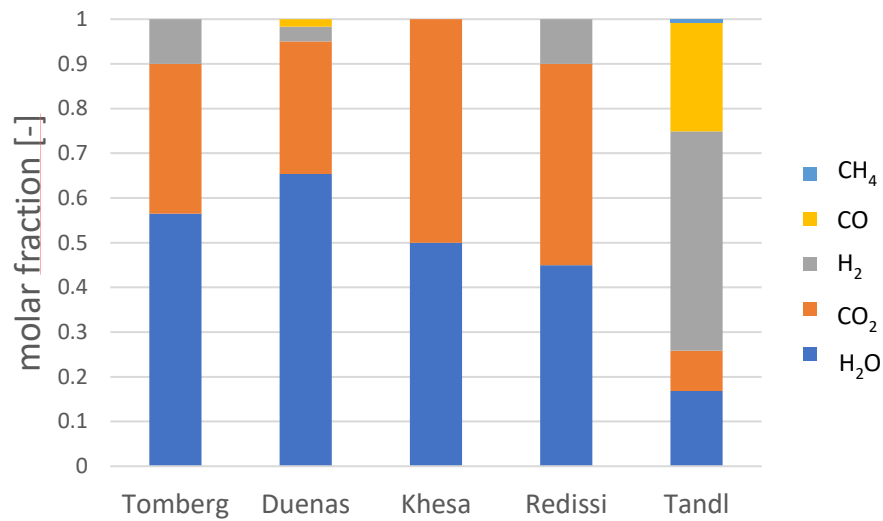
Figure 6 inlet molar fractions of the publications

It is noticeable that in Khesa and Mulopos publication only water and carbon dioxide are added to the electrolysis. These are the primary reactants for co-electrolysis. However, it is advisable to have a hydrogen content of at least 10 % in the feed stream in order to avoid oxidation of the nickel cathode (Fu et al., 2010; Peters et al., 2022). Tomberg and Redissi and Bouallou have similar inlet streams. Dueñas et al. has a high proportion of water (over 65 %), but carbon monoxide and hydrogen only make up 5 % together. Tandls composition differs from the others in that a lot of carbon monoxide and hydrogen are recycled. The products, water and carbon dioxide, make up less than 26 %. Methane is also present with 0.7 %.

With such different operating conditions and inlet flows, different results are to be expected and are analyzed below.

Process simulation

3.1.1.2 Literature results

In Figure 7, the molar fractions at the outlet are shown. A table with the exact values can be found in the appendix (see Table 19).
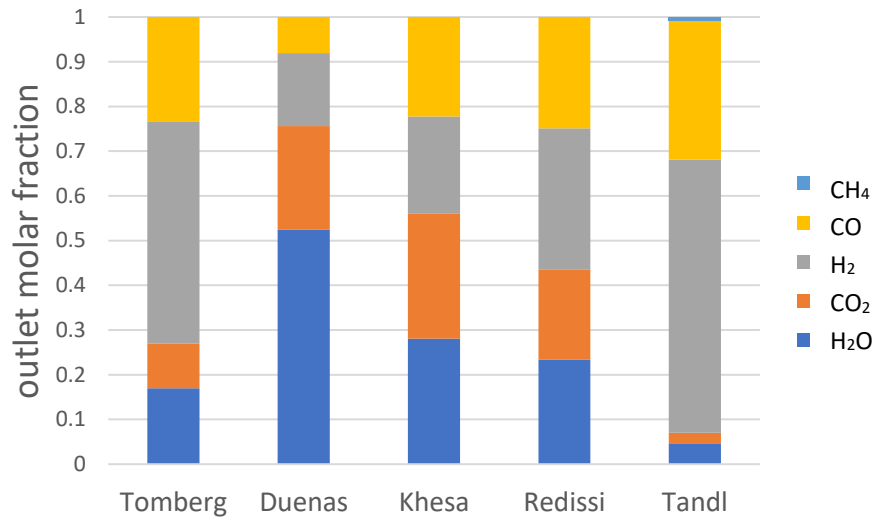
Figure 7 published outlet molar fractions

Dueñas et al. converted only a few educts. The product stream still contains more than 75 % molar fraction of water and carbon dioxide. This is due to the low RU of 20 %. Tomberg has an RU of 70 % and over 70 % molar fraction of syngas in the product stream. Tandl has a very high share of over 90 % hydrogen and carbon dioxide. This is due to the very high proportion of these substances in the educt stream and the high RU of 73 %.

Figure 8 shows the molar ratios of hydrogen and carbon monoxide. They are calculated using the following Formula (17).

$$mr = \frac{x_{H_2}}{x_{CO}}$$

(17)

Process simulation
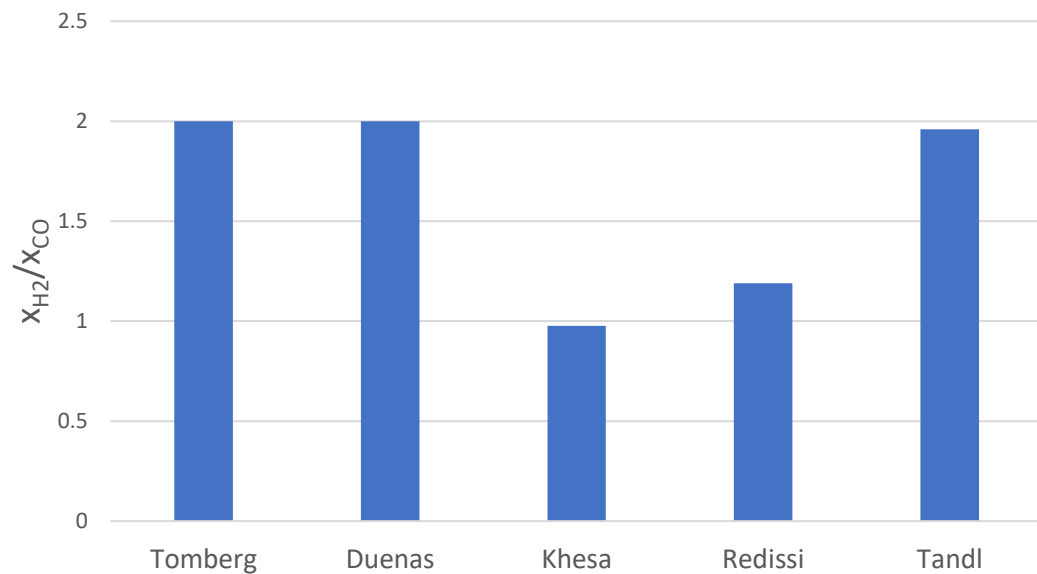
Figure 8 molar ratios literature results

It is noticeable that Khesa and Mulopo has the lowest molar ratio of just under 1, which is partially due to the fact that water and carbon dioxide are present in equal proportions in the feed stream. Khesa and Mulopo has simulated in Aspen Plus with the electrolyzer model 1 (see Figure 9). The composition of the product stream depends mainly on the composition of the feed stream and the RU. Unfortunately, it is not clear from the paper which RUs are used, as different specifications are given. But even if the individual RUs are used for water (0.526) and carbon dioxide (0.3932), they are very similar. Since there is no molar ratio of 1, different RUs must be used for water and carbon dioxide.

Redissi and Bouallou achieves a molar ratio of 1.2, which is due to the similar but not identical RUs and the same proportions of water and carbon monoxide in the feed stream. Tomberg, Dueñas et al. and Tandl reach a molar ratio of exactly or just below 2. Since they all use the same RU for water and carbon dioxide, this is mainly explained by the composition of the inlet feed, where the water content is higher than the carbon dioxide content. In summary, the choice of inlet compositions and RU significantly affects the composition of the product stream.

3.1.2   Aspen electrolyzer models

Khesa and Mulopo used the configuration of a RStoich reactor with a product stream separation (see Figure 9).

Process simulation
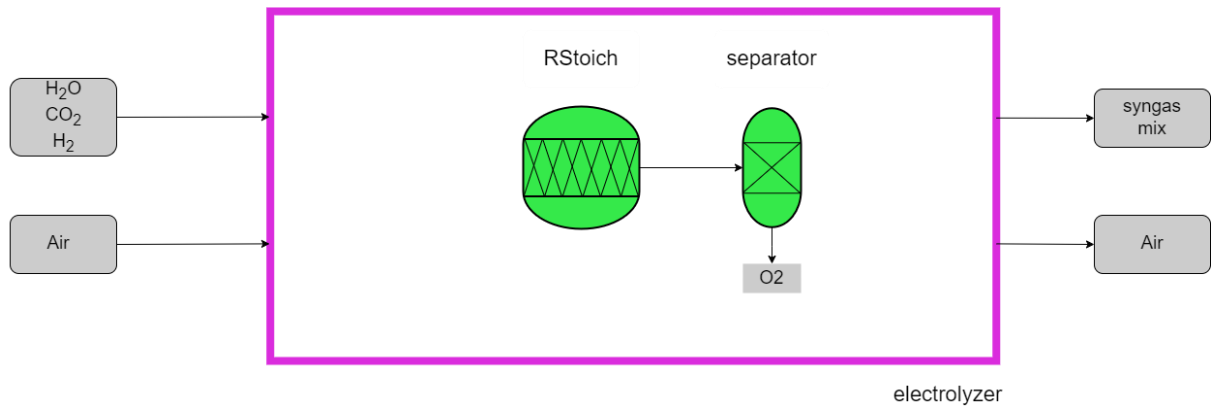
Figure 9 aspen electrolyzer model 1

The stoichiometric reactor calculates the defined reaction enthalpy and entropy based on known and fixed conversion rates of the reactants for a given temperature and pressure. It outputs the heat duty, which represents the enthalpy required to reduce water and carbon dioxide. Dividing this value by the efficiency of the electrolyzer gives the electrical power requirement of the electrolyzer (see equation (18)).

$$P_{el,electrolyzer} = \frac{\Delta h}{\eta_{electrolyzer}} \qquad (18)$$

The separator unit separates the air from the product stream and is needed because the gases come from different electrolyzer compartments. Since the RStoich reactor has only one outlet, the product stream from the reactor must be separated from the electrolysis product stream. However, the work output must be neglected. An advantage of this model, is its simplicity. A disadvantage is that it considers only the reduction reactions in the stoichiometric reactor. The RWGS is neglected.

Process simulation

Redissi and Bouallou used a different reactor configuration. In his publication two additional REQuil reactors are considered (see Figure 10).
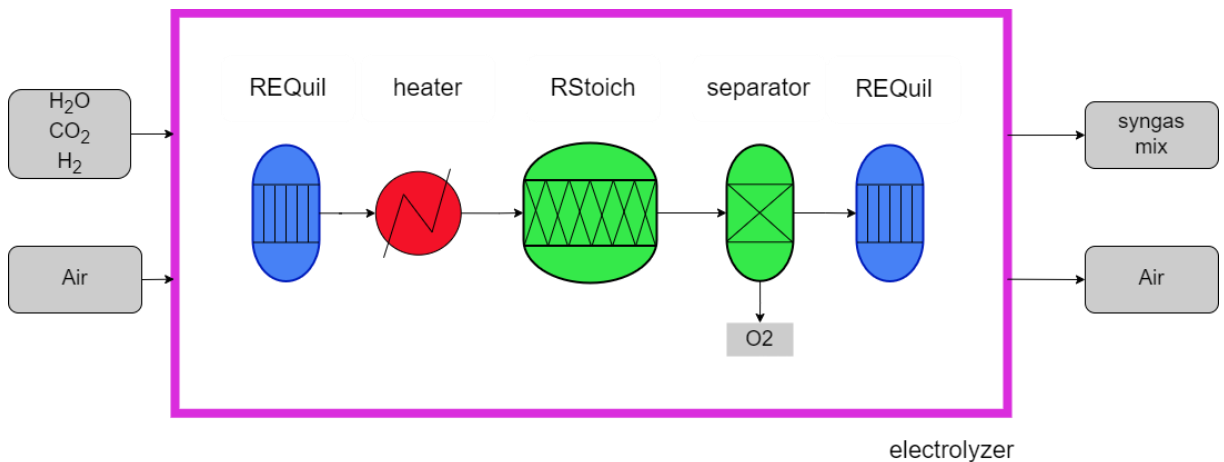
Figure 10 aspen electrolyzer model 2

These equilibrium reactors will simulate the RWGS reaction. As the reduction reactions and the RWGS reaction take place simultaneously, there will be two equilibrium reactors. One before and one after the stoichiometric reactor. The first equilibrium reactor is operated at 200 °C, the second one at the operating temperature of the electrolyzer.
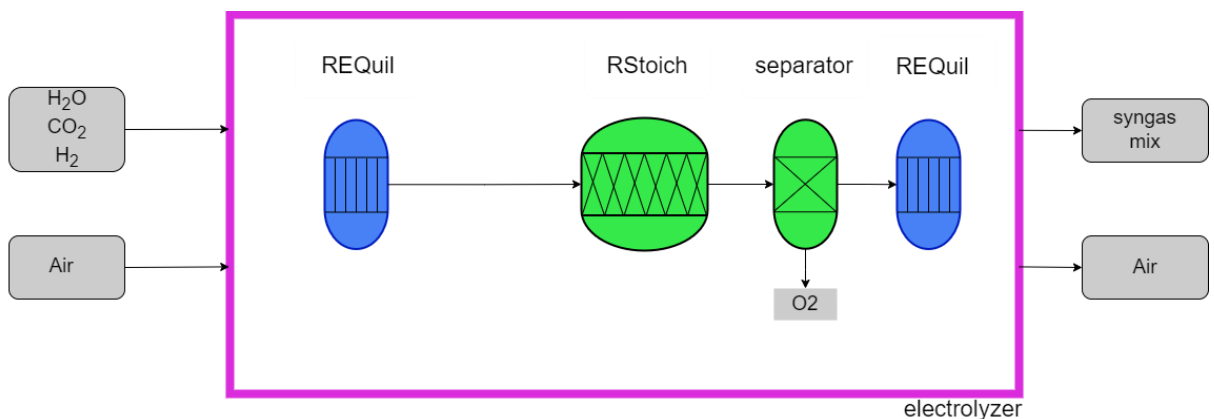
Figure 11 aspen electrolyzer model 3

The plan is to evaporate the water as a pure substance, rather than heating a liquid-gas mixture. When heating a liquid-gas mixture heat transfer is difficult. After the evaporation of the water, the CO_2 is added and superheated together with the water vapor. As mentioned above, hydrogen should be added as late as possible. Therefore, there is no low-temperature RWGS as in model 2. The reactants are combined at the operating temperature of the electrolyzer. Model 3 (cf. Figure 11) has the same components as Model 2, but the first equilibrium reactor is operated at the operating temperature of the electrolyzer.

Therefore, no heater is required between the first equilibrium reactor and the stoichiometric reactor. Model 4 (cf. Figure 12) investigates whether the first equilibrium reactor can be eliminated.
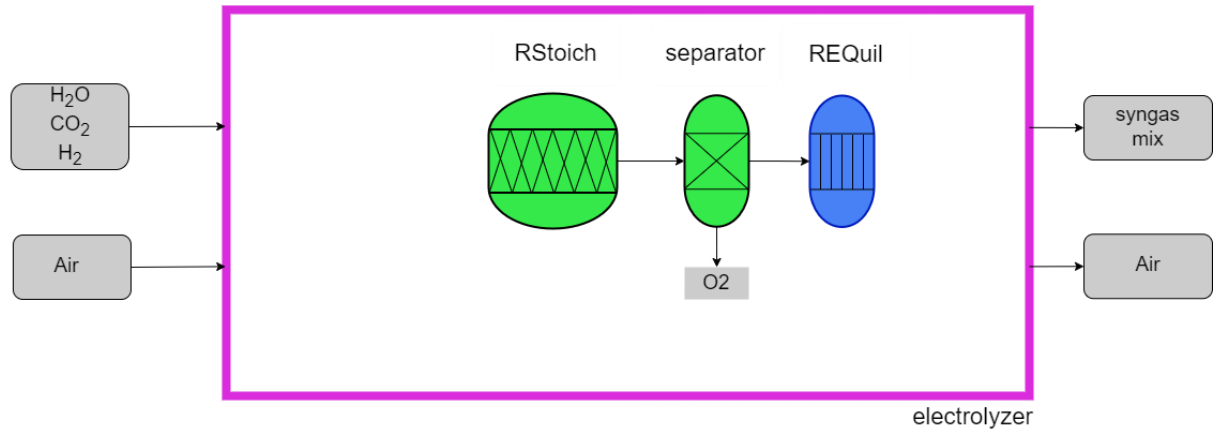
Figure 12 aspen electrolyzer model 4

As mentioned in chapter 2.3.1, there is a possibility of methane formation during the co-electrolysis process. To account for this, the methanation reaction (see Formula (11)) is embedded in the equilibrium reactors of model 2, 3 and 4.

3.1.3   Heat integration

After determining the electrolyzer model, it is possible to investigate how to recover as much heat as possible in the electrolysis process. As shown in Figure 5, a product stream and a stream of air enriched with oxygen leave the electrolyzer. Both streams contain thermal energy that can be recovered. The air stream is used to superheat the incoming air stream and preheat the carbon dioxide stream. For this high-temperature heat exchanger 5, a temperature difference of 50 K is aimed for between the hot inlet and the cold outlet streams. For heat exchanger 6, a temperature difference of 10 K is selected between the hot inlet and the cold outlet streams. Theoretically, these temperature differences are not necessary because all the thermal energy can be transferred, but the heat exchanger must be infinitely long. The larger the heat exchanger, the greater the pressure drop and the more expensive it will be.

It is possible to preheat the hydrogen stream with the remaining heat energy. However, this is technically complicated and expensive due to the volatility of hydrogen (Schmidt, 2022) and is therefore not implemented. Hydrogen is superheated with electrical energy.

Process simulation

The product stream is used to preheat and vaporize the water and to superheat the water/carbon dioxide mixture. For the heat exchanger 7, the temperature difference between the hot outlet and the cold inlet is set to 50 K.

The temperature difference between the hot outlet and the cold inlet of heat exchanger 8 must be approximated. A difference of 10 K as shown in Figure 13 will not work due to the phase change of the water. The hot stream (red line) cannot physically become colder than the cold stream (blue line). However, this is the case due to the partial evaporation of water in the cold stream. The product stream also contains some water that is partially liquefied in the heat exchanger.
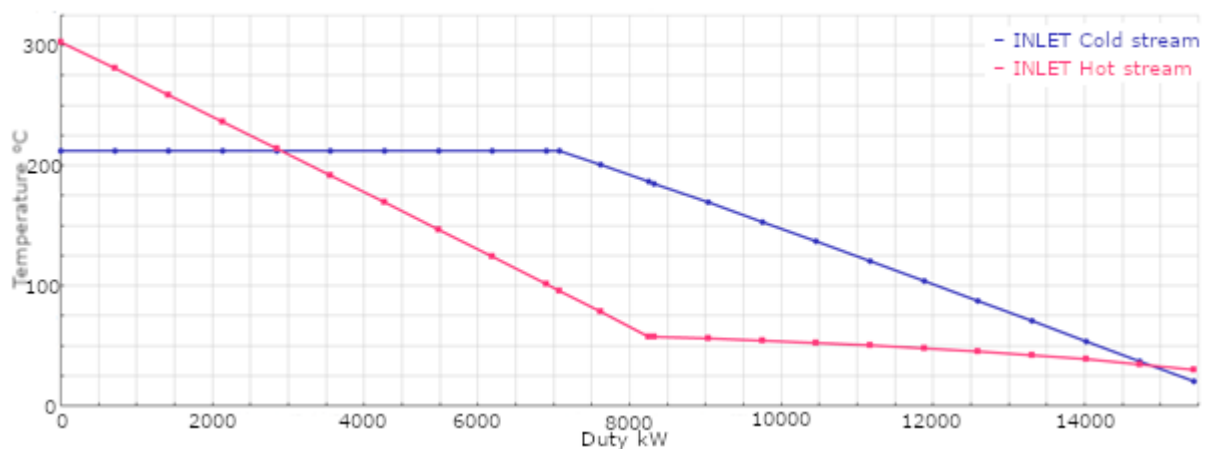
Figure 13 TQ-diagram heat exchanger 8 hot inlet cold outlet temperature difference of 10 K[1]

To make the heat exchanger physically possible, a pitch-point analysis is performed and the temperature difference is increased until a minimum temperature difference of more than 10 K is continuously maintained. This is the case when 35 K is entered as the temperature difference between the cold inlet and hot outlet stream. In this way, the required temperature difference is obtained and as much heat as possible is recovered (see Figure 14).

---

[1] Due to the unavailability of aspen in the final phase of my thesis, Figure 13 and Figure 14 are in low resolution

Process simulation
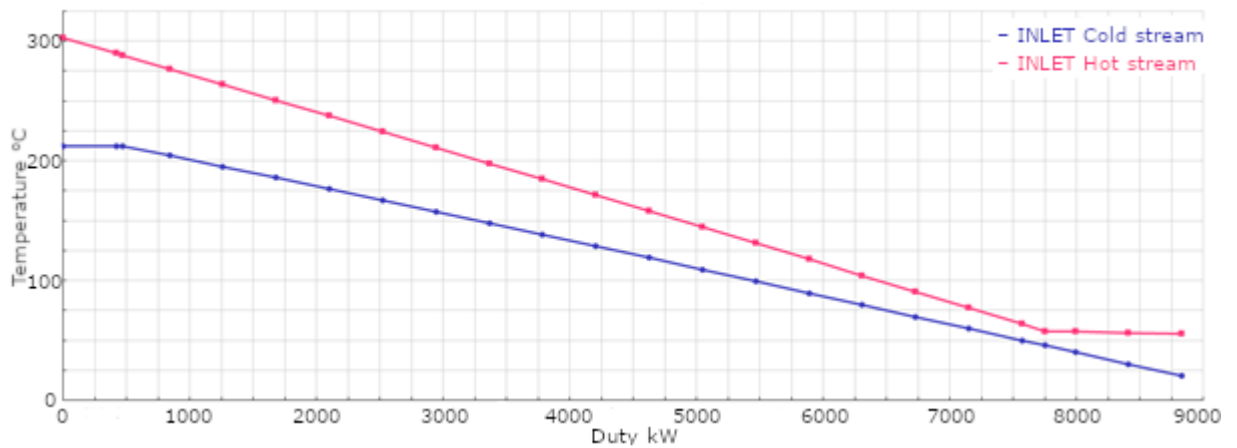
Figure 14 TQ-diagram heat exchanger 8 hot inlet cold outlet temperature difference of 35 K

The energy for the remaining evaporation and superheating of the streams, except for the hydrogen stream, is provided by solar energy.

3.2 Results

The results obtained with the four electrolyzer models and the input data from the five publications are presented and discussed. The simulation results are further compared with the published data. The output composition and chemical power are compared. Based on these results, a decision is made as to which electrolysis model is used. This is validated with experimental data and then simulated in Aspen to obtain specific heat and power requirements.

3.2.1 Simulation results

Based on the literature, four different electrolyzer models for aspen are developed and adapted to the planned operating conditions (cf. chapter 3.1.2). Data from five publications serve as input. Figure 15 shows the molar ratios of hydrogen and carbon monoxide.

Process simulation
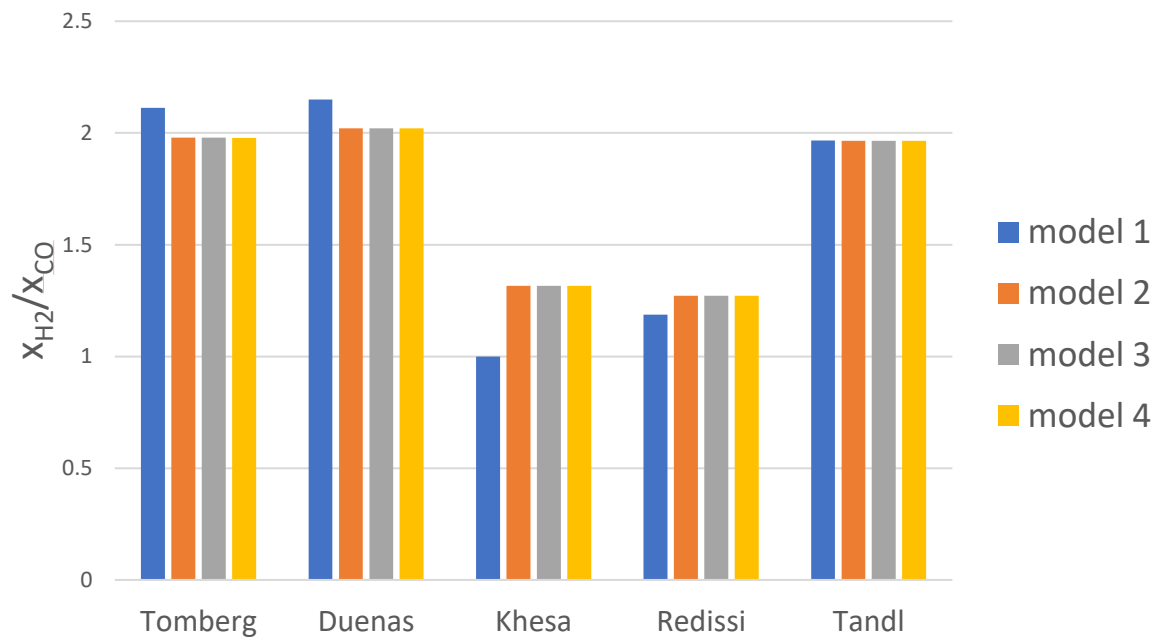
Figure 15 molar ratios from different aspen simulations

The molar ratios are within the range of 1 to 2.1. It is noticeable that models 2 to 4 do not show any differences. Model 1 is sometimes above models 2, 3 and 4 and sometimes below.

In the simulations with Dueñas et al. and Tombergs input data, four and three substances involved in electrolysis are present in the inlet flow, respectively. The operating temperatures are 830 and 825 °C. This indicates that the RWGS reaction is taking place and the equilibrium is on the side of water and carbon dioxide. This means that hydrogen is consumed and more carbon monoxide is produced. Therefore, the molar ratio for Tomberg and Dueñas et al. is higher in Model 1. Because there is no RWGS reaction in Model 1, the outlet stream contains more water and less carbon monoxide. It makes a difference whether the equilibrium reaction is included or not. However, it is not clear whether it makes a difference how many equilibrium reactors are used and at what temperatures they are operated.

Figure 16 shows the chemical power requirements of the electrolyzer for the different models. The simulations with the values of Tomberg, Redissi and Bouallou and Tandl show small deviations between the individual models, with Model 3 of Tomberg and Redissi and Bouallou and Model 1 of Tandl deviating the most from the other three models.

Process simulation
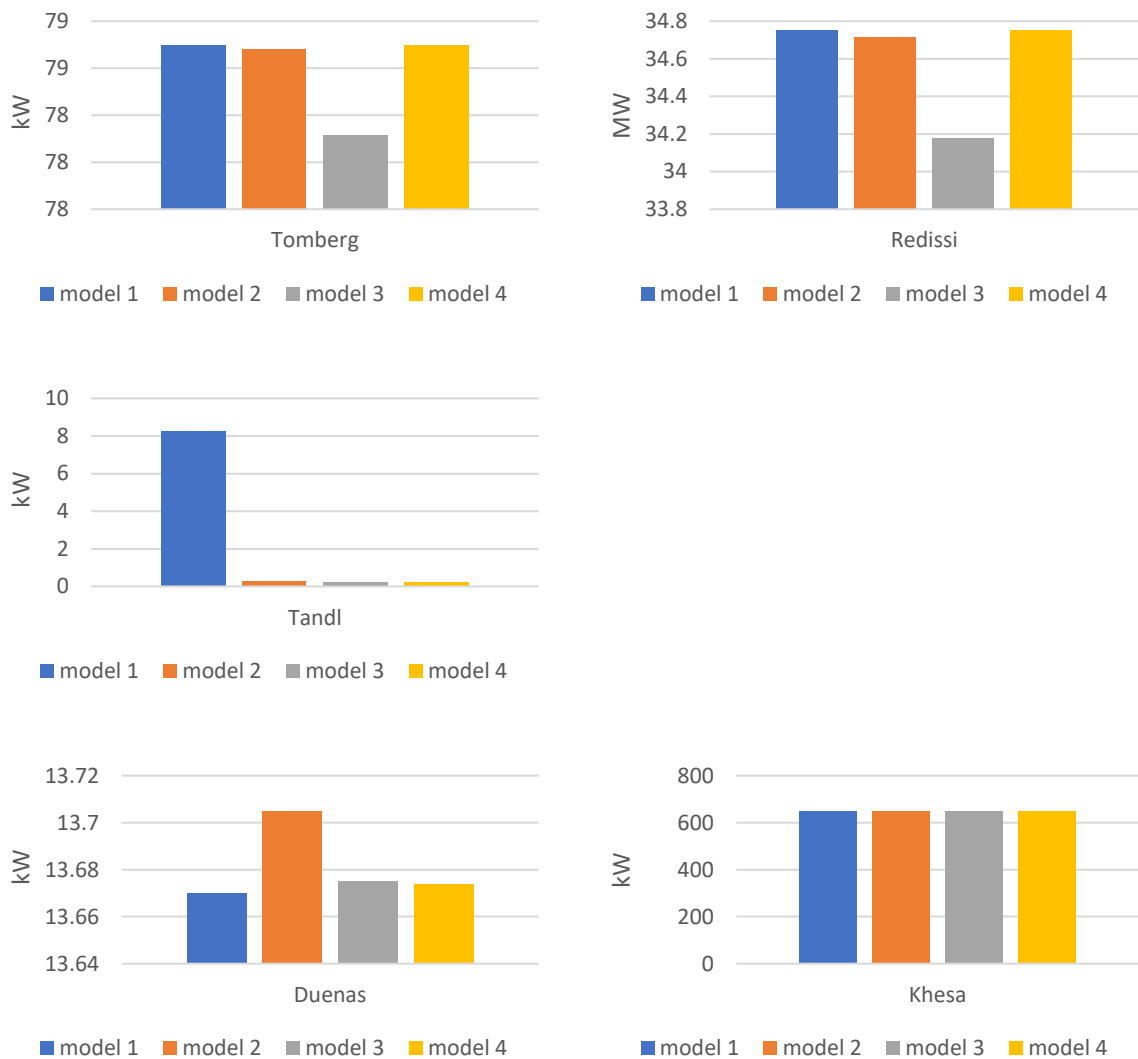
Figure 16 chemical power requirements

When the simulation is done with Dueñas et al. values, there is little difference between the models. In the case of Khesa and Mulopo, there is no difference at all. In models 2 and 3, the RWGS reaction takes place in an equilibrium reactor before the stoichiometric reactor. However, this cannot happen because only carbon dioxide and water are present in the inlet stream and available as reactants. Thus, the same results are obtained with all four models. The equilibrium reactor after the stoichiometric reactor (REQuil reactor 1 for model 4 and REQuil reactor 2 for models 2 and 3) operates at 700 °C. The simulation results show that the molar flows of carbon monoxide and water decrease and those of hydrogen and carbon dioxide increase (see Table 3).

Process simulation

Table 3 Khesa mole flows before and after second equilibrium reactor

mole flow [kg/hr]	before	after
H_2O	5.65	4.99
CO_2	5.54	6.19
H_2	4.36	5.01
CO	4.46	3.81

Hence, at an operating temperature of 700 °C, the equilibrium of the RWGS reaction is on the side of the educts (H_2 and CO_2). Thus, more hydrogen is produced. This explains the higher molar ratio of water to carbon dioxide in Figure 15.

3.2.2   Comparison simulation results with literature

The simulation results are compared with literature data to see which model achieves the best convergence to the results in the papers. The key results of electrolysis are the composition of the output and the electrical power requirement. A comparison of these values is shown below.

3.2.2.1   Outlet composition comparison

The mass flows of the individual substances present in the product stream are used to compare the outlet compositions. In the product stream after electrolysis, the two syngas products hydrogen and carbon monoxide and the two feed materials water and carbon dioxide are present. The publications of Dueñas et al., Khesa and Mulopo and Tandl contain sufficient data to be able to compare them with the simulation data. The relative deviations of the mass flows of the simulation are compared with the mass flows of the publication. Formula (19) shows the calculation for water.

$$f_{H_2O} = \left(\frac{\dot{m}_{H_2O,simulation} - \dot{m}_{H_2O,literature}}{\dot{m}_{H_2O,literature}} \right) \tag{19}$$

Figure 17 to Figure 20 show the relative deviations of the simulation results from the published data for water, carbon dioxide, hydrogen, and carbon monoxide. Depending on the mass flows and models, positive or negative deviations result. A negative deviation means that a lower mass flow of the material has been simulated compared to the published data.

Process simulation
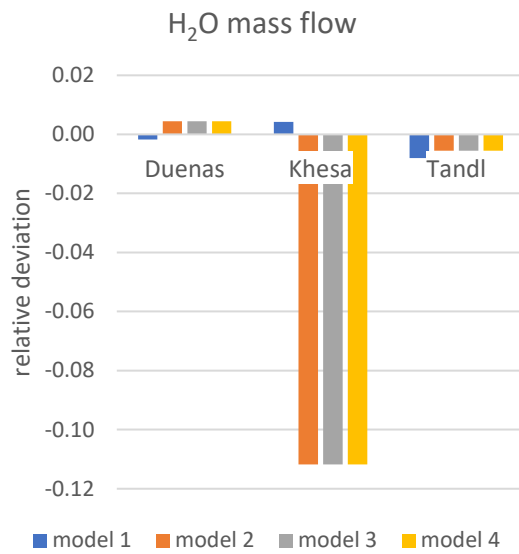
H₂O mass flow

Figure 17 outlet mass flow comparison water
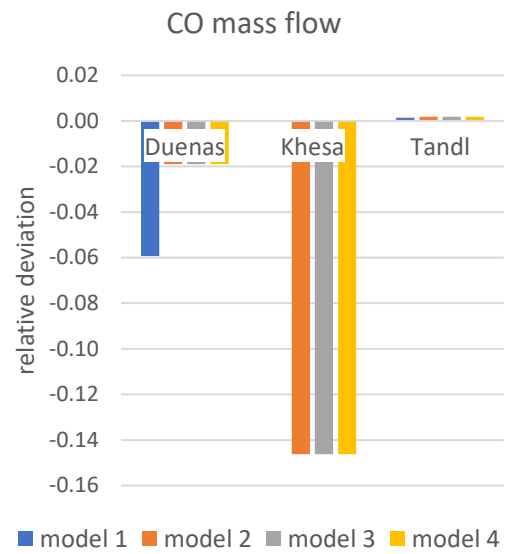
CO mass flow

Figure 18 outlet mass flow comparison carbon monoxide
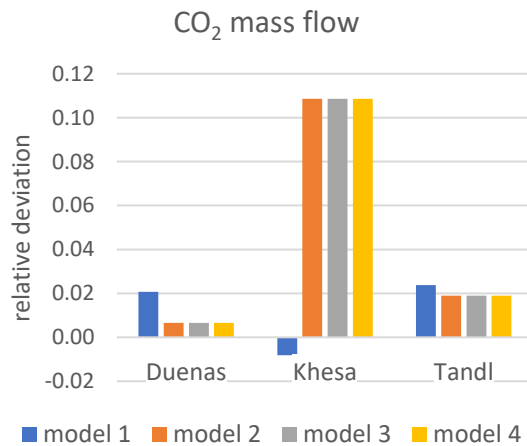
CO₂ mass flow

Figure 19 outlet mass flow comparison carbon dioxide
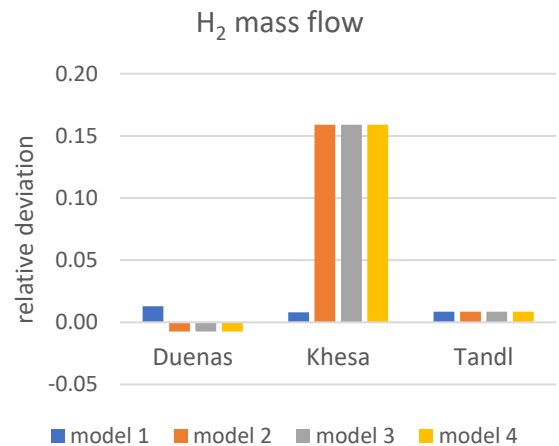
H₂ mass flow

Figure 20 outlet mass flow comparison hydrogen

It can be seen that models 2 to 4 show negligible differences. Model 1 deviates from the other models. With Khesa and Mulopos data, the largest discrepancies are found for models 2 to 4. This can be explained by the fact that Khesa and Mulopo simulated in Aspen using Model 1. Deviations are to be expected. The differences in Model 1 can be attributed to different versions of Aspen and the fact that the paper does not indicate which RU was used. Using Tandls data, all four models show very similar deviations from the literature, both in terms of amount and sign. Using Tandls and Khesa and Mulopos data, the carbon monoxide stream shows the smallest deviations of only 0.1 % and 0 %, respectively. Dueñas et al. has the smallest deviation for water (-0.18 %). For Models 2 to 4, the signs of water and

Process simulation

hydrogen are exactly reversed. For Khesa and Mulopo and Tandl, the product stream in the simulation contains more hydrogen and less water than in the publication.

Unlike the publications, the simulation models take the methanation reaction into account. For model 3, the outlet mole fractions are shown in Table 3. Very little methane is produced. Even with Khesa and Mulopos input values and a rather low temperature of 700 °C, methane has a mole fraction of only 0.11 %. At planned operating temperatures of around 800 °C, methane has an even lower mole fraction of less than 0.05 %. With Tandls input data, methane has an output mole fraction of 0.64 %. This value differs from the others because methane is already present in the input stream.

Table 4 outlet mole fraction with methane reaction

outlet mole fraction	Tomberg	Dueñas et al.	Khesa & Mulopo, 2021	Redissi & Bouallou, 2013	Tandl, 2023
H_2O	18.06%	52.65%	25.18%	23.48%	4.83%
CO_2	9.01%	23.35%	31.21%	20.23%	2.58%
H_2	48.41%	16.05%	24.73%	31.50%	60.94%
CO	24.47%	7.95%	18.79%	24.77%	31.00%
CH_4	0.05%	0.00%	0.09%	0.02%	0.64%
temperature	830 °C	860 °C	700 °C	800 °C	812 °C

3.2.2.2   Power comparison

Aspen's stoichiometric reactor calculates the enthalpy difference of the reactants. This chemical (chem) power is a measure of the electrolyzer's power. In most publications, only the electrical power requirement is given. This can refer to the electrical power requirement of the reactor only (Formula (20)) or to the whole system (Formula (21)).

$$P_{el,reactor} = \frac{P_{chem}}{\eta_{reactor}} \tag{20}$$

$$P_{el,system} = P_{el,reactor} + P_{compressors} + P_{pumps} + P_{heater} \tag{21}$$

No information is given on the efficiency of the reactor or on the energy requirements of the pumps, compressors and electric heaters. Therefore, it does not seem reasonable to compare the chemical performance of the aspen simulation with the electrical energy requirements of the publications. Tomberg gives a chemical energy requirement in his publication. This is compared with the simulation results (see Formula (22)).

Process simulation

$$f = \frac{P_{chem,published,Tomberg}}{P_{chem,simulation}} \qquad (22)$$

The relative agreement of the two energy requirements is shown in Figure 21. The higher the value, the more the two values match.
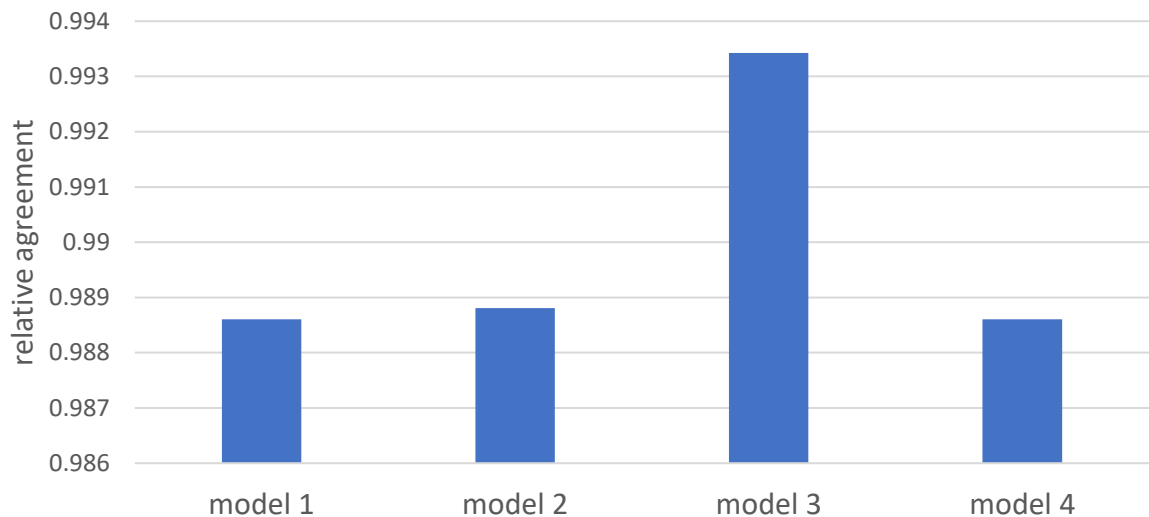
Figure 21 chemical power comparison simulated values and published values from Tomberg

Models 1, 2 and 4 have similar agreement of 98.8 to 98.9 %. Model 3 achieves over 99 % agreement between simulated and published chemical power values. Since Model 3 shows the best agreement with the published data, this model is further investigated.

Both Dueñas et al. and Tandl have experimental data for the co electrolysis. In the following, the simulation results of Model 3 are compared with the experimental data of the two publications in order to validate the model.

3.2.3   Comparison simulation results Model 3 with experimental data

Dueñas et al. goal is the electrochemical reduction of water and carbon dioxide, to provide a suitable composition for subsequent processes. Figure 22 shows the outlet mole flows in kg/hr.

Process simulation
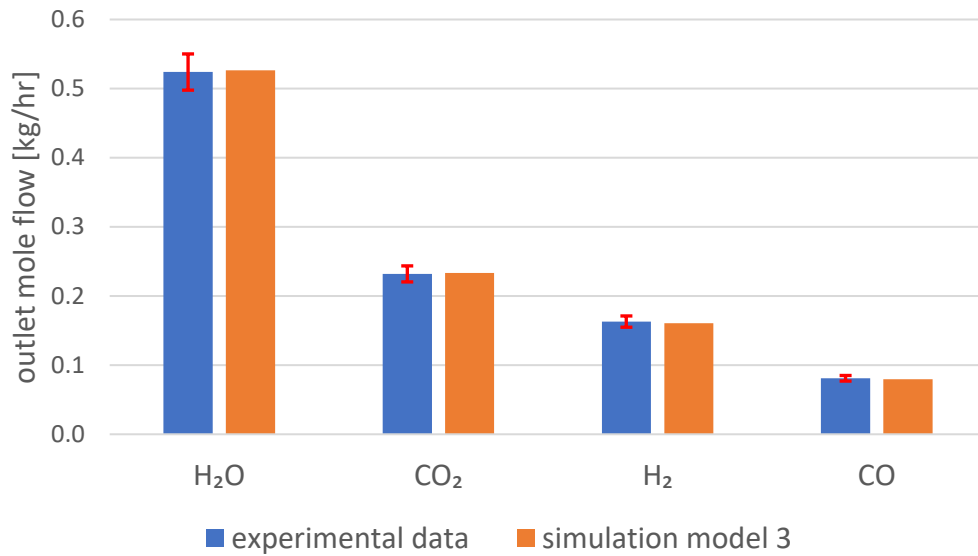
Figure 22 outlet mole flow comparison simulation model 3 and experimental data from Dueñas et al.

The experimental data from Dueñas et al. are shown in blue, and the simulation results from Model 3 are shown in orange. A 5 % uncertainty is indicated in red. The differences are very small. The deviations are all less than 5 %.

Tandls publication describes the development of a highly efficient power-to-liquid plant based on co-solid oxide electrolysis. Experimental results are obtained using a 10-cell test. Fig. 4 shows the outlet volume flow from the experimental data from Tandl and the simulation Model 3 in m³/hr. An uncertainty of 5 % is again marked in red.
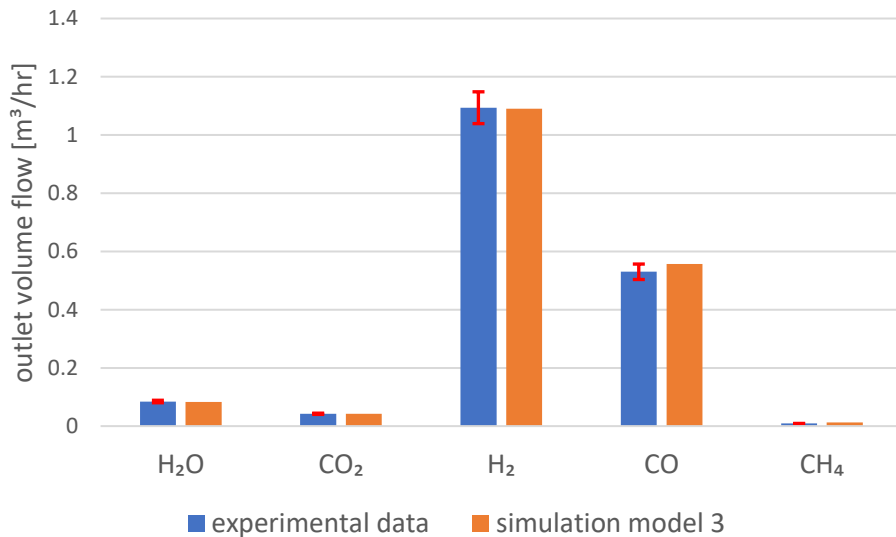
Figure 23 outlet volume flow comparison simulation model 3 and experimental data from Tandl

Process simulation

Again, the deviations between simulated and measured data are less than 5 %. These results look very promising and validate the electrolyzer Model 3. The co-electrolysis process is simulated in aspen with a stoichiometric reactor and a pre- and post-equilibrium reactor. All reactors are operated at the same temperature (cf. Figure 11). Based on Figure 5 the electrolysis model can now be implemented into the complete process in aspen.

3.2.4   Complete co-electrolysis process in aspen

Figure 24 shows the complete aspen electrolysis process. Starting from 20 °C, air, hydrogen and carbon dioxide must be superheated and water must be evaporated and superheated. As much heat as possible is recovered from the exhaust air stream and the syngas stream.

Process simulation

Figure 24 complete electrolysis model in aspen

Process simulation

Important operating conditions are listed in Table 5 and Table 6. The specific thermal and electrical energy requirements can be calculated using Formula (23). They refer to the syngas mole flow.

$$q = \frac{Q}{\dot{n}_{syngas}} \qquad\qquad (23)$$

Table 5 mole fractions and flow rate aspen simulation

Indicators	Units	inlet	outlet
Mole fraction H_2O	%	56.5	17.92
Mole fraction CO_2	%	33.5	9.17
Mole fraction H_2	%	10	48.54
Mole fraction CO	%	0	24.31
Mole fraction CH_4	%	0	0.06
Molar flow rate	kmol/sec	1	1

Table 6 operating conditions aspen simulation

Indicators	Units	
electrolyzer temperature	°C	820
electrolyzer pressure	bar	1
RU	%	70
Specific thermal energy demand (heater water evaporation, H2O, CO2 super heating, air super heating)	kWh/kmol	46.88
Specific electrical energy demand (water pump, air compressor, hydrogen heater,electrolyzer)	kWh/kmol	300.69

For further consideration, the specific electrical and thermal energy requirements are of particular importance. Thermal energy is required by heaters 1, 2 and 3. Electrical energy is required by the water pump, the air compressor, the electrical heater of the hydrogen flow, the separator for the water and the syngas mixture, and the electrolyzer. The pump compresses the water from 1 to 20 bar for vaporization. After evaporation, the steam is depressurized to 1 bar with valve B10. The air compressor compresses the air to 1.5 bar. For the carbon dioxide and hydrogen flow, it is assumed that both substances are stored in compressed form and therefore no compressor needs to be considered. As mentioned above, hydrogen is electrically superheated due to its volatile nature. The energy demand of the electrolyzer is calculated from the energy consumption of the two equilibrium reactors and the stoichiometric reactor.

4   Transient load and thermal storage integration analysis

The following chapter examines the energy and mass balances of key components. To ensure continuous operation, the use of a thermal energy storage system is investigated. An existing Python model for steam electrolysis is used and adapted to the co-electrolysis process. The source code for the variable definition and the efficiency of the solar field was reused. These basics were provided by the German Aerospace Center. Various process operation modes are analyzed and the results are presented.

In the planned co-electrolysis process, concentrated solar energy is used to heat the mass flows required for the co-electrolysis to over 800 °C. Air, carbon dioxide and water flow through a receiver and are evaporated (eva) or superheated (sup).

4.1   Receiver power

Solar energy is not available all the time or at the same intensity. A typical load pattern for one day of the year for the DNI for Ouarzazate is shown in Figure 25.
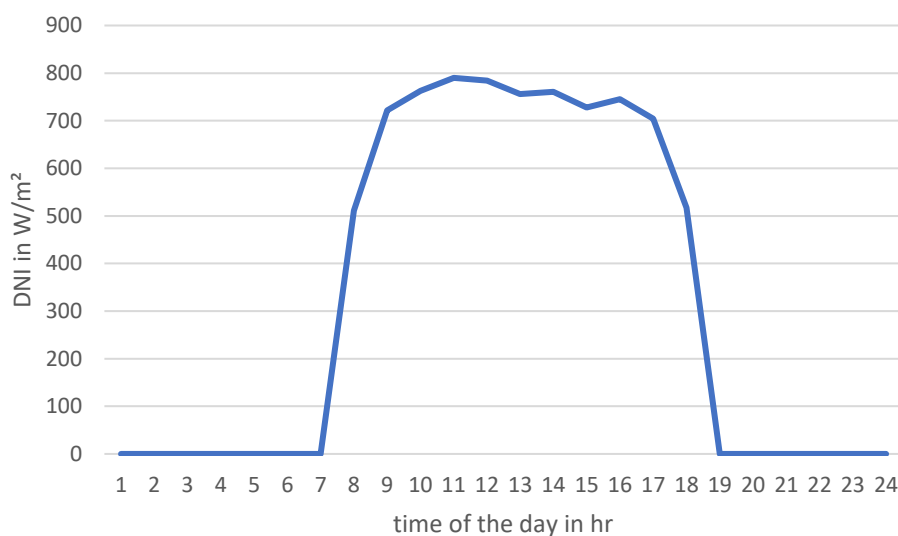
Figure 25 DNI on 21. March in Ouarzazate

Solar radiation varies according to the season and time of day. To determine the appropriate thermal and electrical energy requirements for the co-electrolysis process, an annual syngas production rate estimation is performed. The year is divided into 8760 hours. For each hour the corresponding energy demand is calculated depending on the receiver power.

For the electrolysis process temperatures above 800 °C are required. For the evaporation of the water, lower temperatures are sufficient. Therefore, the idea is to implement a high (HT) and a low temperature (LT) thermal energy storage. A latent thermal energy storage is used

Transient load and thermal storage integration analysis

as the low temperature energy storage. A sensitive storage is used as the high temperature energy storage. In this paper, storage is only considered in terms of energy power and storage capacity. The state of charge (SOC) refers to both storage tanks equally.

The receiver power can be calculated using the following Formula (24).

$$\dot{Q}_{Receiver} = \eta_{receiver} \cdot \dot{Q}_{Intercept} \tag{24}$$

The intercept power can be calculated with Formula (27). Information on the receiver efficiency and the size of the heliostat field can be found in Table 7 .

$$\dot{Q}_{Intercept} = \eta_{SF} \cdot DNI(t) \cdot A_{Heliostat} \tag{25}$$

The solar DNI data comes from Meteonorm, the receiver efficiency is assumed, the solar field efficiency depends on the DNI and is recalculated for each time step.

Table 7 boundary conditions

Indicators	Units	
location	-	Ouarzazate
$\eta_{receiver}$	-	0.9
$\eta_{electrolyzer}$	-	0.972 (Tomberg et al., 2023)
$A_{Heliostat}$	m²	160,884.4

With the energy demand calculated in Aspen, it is possible to calculate how the receiver power is split among the three streams (H2O_eva, H2OCO2_sup and Air) (cf. Formula (26)).

$$f_i = \frac{\dot{Q}_i}{\dot{Q}_{HX1} + \dot{Q}_{HX2} + \dot{Q}_{HX3}} \tag{26}$$

As shown in Table 8, more than three-quarters of the energy is required to evaporate water. The energy referred to here applies only to the input data listed in Table 5 and Table 6.

Table 8 Receiver power from aspen simulation

	power	relative proportion
HX1(H2O_eva)	19,978 kW	0.0638
HX2 (H2OCO2_sup)	4,588 kW	0.1748
HX3 (Air)	1,675 kW	0.7613
Receiver	26,241 kW	1

4.2 Energy and mass balances

Energy and mass balances for the three heat exchangers required to heat the streams are shown in Figure 26. The red rectangles on the left represent the initial materials. In this case, the mass and composition do not change. They are heated. The water changes its state. The heat exchangers receive their energy from the receiver.

Transient load and thermal storage integration analysis
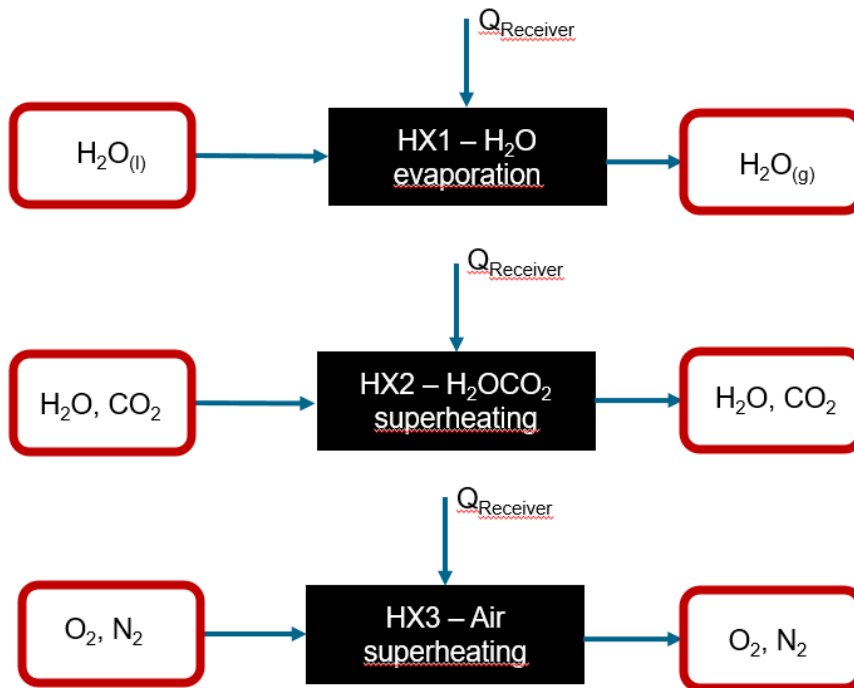
Figure 26 energy and mass balances heaters
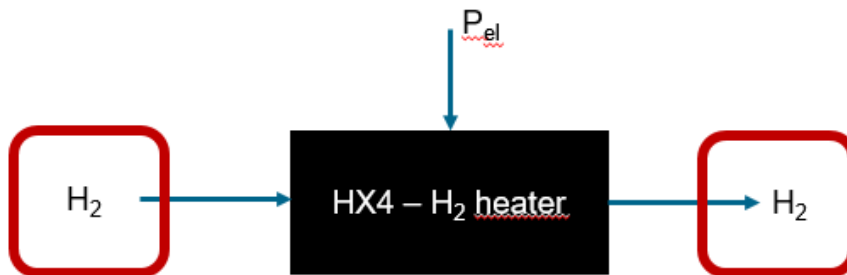
Figure 27 energy and mass balances heater hydrogen

Figure 27 shows the energy and mass balance for the hydrogen heater. This heater is powered by electrical energy.

The energy and mass flows for the electrolyzer are shown in Figure 28. The red box on the left shows the input materials. The black box in the middle represents the electrolysis process. The arrows show the material and energy flows. The electrolysis process is supplied with electrical energy. The thermal energy required for electrolysis is carried by the material streams.

Transient load and thermal storage integration analysis
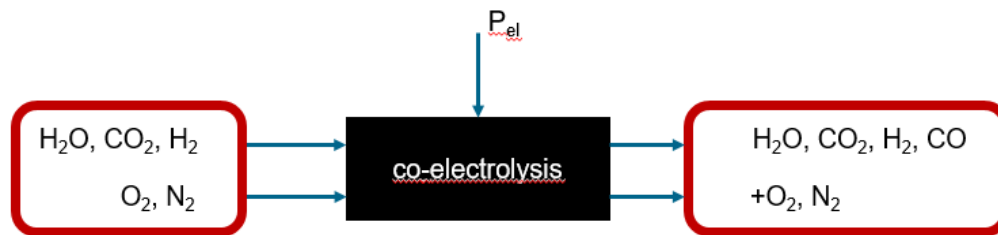
Figure 28 energy and mass balance co-electrolysis

4.3 Different operating modes

Eight different operating modes have been identified. The following questions can be asked. Is there enough solar power to operate the electrolyzer at nominal power? Can the thermal energy storage be charged? Does the thermal energy storage need to be discharged? Is the state of charge sufficient to discharge the thermal energy storage? Do parts of the electrolyzer need to go into standby or does the entire electrolyzer need to go into standby? Depending on the case, the electrolyzer will have different powers available and different mass currents will flow through the receiver. This chapter starts with the calculation for some required values. Then the control algorithm for cases 1 to 4 and cases 5 to 8 is explained.

4.3.1 Calculation and values needed for control algorithm

Required specific values are listed in Table 9 and are calculated according to the same principle as Formula (23).

Table 9 specific values

Indicators	Related to mole flow	Units	specific power
$p_{water,pump}$	Water	kWh/kmol	0.01180
$p_{air,comp}$	Air	kWh/kmol	0.3636
q_{heater,H_2}	Hydrogen	kWh/kmol	6.5694
p_{syngas}	Syngas	kWh/kmol	294.1

The specific electrical energy required to heat the hydrogen is calculated by multiplying q_{heater,H_2} by an assumed efficiency of 0.9.

The specific thermal energy requirement of the high temperature electrolyzer (HTE) can be calculated with Formula (27).

Transient load and thermal storage integration analysis

$$\frac{\dot{Q}_{HTE}}{P_{HTE}} = \frac{26{,}241 \text{ kW}}{164{,}626 \text{ kW}} = 0.15940 \tag{27}$$

This value is performance independent. The storage capacity and the nominal electrical energy demand of the electrolyzer are calculated using formulas (28) and (29).

$$Q_{TES,max} = Q_{Nominal} \cdot t_{TES} \tag{28}$$

$$P_{HTE,Nominal} = \frac{P_{chem}}{\eta_{electrolyzer}} \tag{29}$$

To calculate the mass flows of the receiver streams, the energies of the streams are required. These can be calculated by multiplying the relative proportions from Table 8 by the receiver energy. The mass flows can then be calculated using the following Formula (30).

$$\dot{m}_i = \frac{Q_i \cdot 3600 \text{ h}}{\Delta h_i} \tag{30}$$

The hydrogen flow rate is calculated from the ratio of hydrogen to the water/carbon dioxide mixture, which is flowing through the electrolyzer. This value is 0.9. This means that the electrolyzer must be supplied with 8 times the molar flow of the water/carbon dioxide mixture as hydrogen. Formula (40) shows the calculation.

$$n_{H2,feed} = n_{H2OCO2,sup,HTE} \cdot frac_{H2OCO2\_to\_H2} \tag{31}$$

The storage discharges itself with time. This self-discharge is calculated with the SOC (see Formula (41)). x_{sf} is the fraction of storage that is discharged per hour. It is calculated using formula (42).

$$SOC_{TES}(t) = SOC_{TES}(t-1) \cdot x_{SF} \tag{32}$$

$$x_{sf} = 1 - \frac{0.5}{24} \tag{33}$$

For the standby mode, a value is needed that indicates how much energy the electrolyzer needs in standby mode. In Tombergs paper, there is information on the electrical system energy consumption and the electrical energy required in standby. Dividing these values gives a standby (SB) value depending on the electrical power (see Formula (43)).

$$x_{SB} = \frac{6.5 \text{ kW}}{91.5 \text{ kW}} = 0.071 \tag{34}$$

The control algorithm is described in the following.

Transient load and thermal storage integration analysis

4.3.2   Case 1 to 4

The input data of the algorithm are

- DNI
- Intercept power
- Thermal energy storage time
- electrical energy demand of the electrolyzer

An overview of the algorithm is illustrated in Figure 29.

The process begins by verifying that there is sufficient receiver energy to operate the electrolyzer. This is the case when the receiver energy is sufficient to superheat the mixture of water and carbon dioxide as well as the air. This requirement is checked using the following Formula (35).

$$Q_{Receiver} \geq Q_{H_2O,CO_2,sup,max} + Q_{air,max}$$

(35)

If sufficient energy is available, it is checked whether the receiver energy is sufficient to operate the electrolyzer at full load. If the receiver energy is equal to the nominal energy, case 3 occurs. The solar energy is sufficient to heat all three receiver currents. The electrolyzer is operated at full load, the storage is neither charged nor discharged. The same conditions (case 2) apply when more receiver energy is available than the nominal energy, but the storage is already full and cannot be loaded with more energy. In this case, more energy is available than is needed. The surplus energy is calculated with Formula (36).

$$Q_{too\_much} = Q_{Receiver} - Q_{HTE}$$

(36)

The query as to how full the storage is, is made via the SOC. This value is set to zero at the beginning of the program and then recalculated for each time step. The value can vary between 0 and 1. In case 2 the SOC of the thermal energy storage is 1. In case 3, the SOC remains the same as in the previous time step. The storage is considered full at a SOC of 0.99 to prevent rounding errors.

If there is more energy available than the electrolyzer needs under nominal conditions and the storage is not fully charged, case 1 occurs. The electrolyzer is operated at full load and the storage is charged. The charge current is calculated as the difference between the receiver energy and the electrolyzer capacity (see Formula (37)).

$$Q_{TES,C} = Q_{Receiver} - Q_{HTE}$$

(37)

Transient load and thermal storage integration analysis

The solar energy is sufficient to heat all receiver streams and to charge (C) the storage. If the storage is so full that it would be overcharged in the next time step (Formula (38)), the charging energy for this hour is smaller (Formula (39)).

$$\frac{Q_{TES,C}}{Q_{TES,max}} > (1 - SOC_{TES}) \tag{38}$$

$$Q_{TES,C} = (1 - SOC_{TES}) \cdot Q_{TES,max} \tag{39}$$

In this hour, more energy is available than can be consumed. The surplus energy is calculated in this case according to the Formula (40).

$$Q_{too\_much} = Q_{Receiver} - Q_{HTE} - Q_{TES,C} \tag{40}$$

If the receiver energy is not sufficient to operate the electrolyzer at full load, it is checked whether the storage can be discharged. For this purpose, the charging capacity is calculated as a function of the SOC (see Formula (41)).

$$Q_{TES} = Q_{TES,max} \cdot SOC_{TES} \tag{41}$$

If the sum of the charge and receiver energy is greater than or equal to the electrolyzer's nominal energy, case 4 applies (see Formula (42)).

$$Q_{TES} + Q_{Receiver} \geq Q_{Nominal} \tag{42}$$

The electrolyzer can be operated under nominal conditions. As can be seen in Formula (43) the discharge (D) energy is the difference between the electrolyzer energy and the receiver energy.

$$Q_{TES,D} = Q_{HTE} - Q_{Receiver} \tag{43}$$

The new SOC is calculated as follows (Formula (44)).

$$SOC_{TES}(t) = SOC_{TES}(t - 1) - \frac{Q_{TES,D}}{Q_{TES,max}} \tag{44}$$

4.3.3   Case 5 to 8

If the storage's discharge energy and the receiver's energy are not sufficient to operate the electrolyzer at full load, it is switched to partial load operation. This is achieved by switching some stacks of the electrolyzer to standby. The other stacks continue to operate normally. The number of stacks that go into standby depends on how much energy can be discharged from the storage. The discharge energy is calculated using Formula (41). The electrolyzer energy is calculated from the receiver energy and the charge energy (see Formula (45)).

Transient load and thermal storage integration analysis

$$Q_{HTE} = Q_{Receiver} + Q_{TES} \tag{45}$$

The standby portion is calculated from the electrolyzer energy and the rated energy (see Formula (46)

$$f_{part,SB} = 1 - \frac{Q_{HTE}}{Q_{Nominal}} \tag{46}$$

The standby power is provided by electricity and is calculated using Formula (47).

$$P_{HTE,part,SB} = P_{HTE,Nominal} \cdot f_{part,SB} \cdot X_{SB} \tag{47}$$

The electrical power requirement for the electrolyzer in case 5 is calculated using Formula (48) (the number is the specific thermal energy requirement of the electrolyzer (see Formula (27)).

$$P_{HTE} = \frac{Q_{HTE}}{0.1594} \tag{48}$$

The discharge energy is the difference between the energy of the electrolyzer and the energy of the receiver (see Formula (43)). If the storage is so empty that the SOC would go below zero in the next step (see Formula (49)), the discharge energy is calculated with Formula (50).

$$\frac{Q_{TES,D}}{Q_{TES,max}} > SOC_{TES} \tag{49}$$

$$Q_{TES,D} = SOC_{TES} \cdot Q_{TES,max} \tag{50}$$

If the SOC of the storage drops to 0.001 or below, the SOC is set to zero and no energy can be discharged from the storage. The storage is considered empty at a SOC of 0.001 to prevent rounding errors.

If the receiver energy is not sufficient to superheat the water/carbon dioxide mixture and the air, the algorithm checks if there is enough storage energy to run the electrolyzer at full load. This is checked using Formula (51).

$$\left(SOC_{TES} - \frac{Q_{Nominal}}{Q_{TES,max}} \right) > 0 \tag{51}$$

If this is the case, case 6 applies. The electrolyzer is working at full load and the discharge energy is equal to the electrolyzer energy. The SOC is calculated using Formula (44). There is no need to check whether the SOC could fall below zero in the next time step. This is already checked in Formula (51).

Transient load and thermal storage integration analysis

If the storage capacity is not sufficient for full load operation, it is checked whether the storage capacity is sufficient for part load operation. In this case, the same conditions apply as in case 5.

The last possibility is case 7. In this case there is not enough receiver energy and not enough storage energy. The electrolyzer energy is zero. The standby power of the electrolyzer is provided electricity. It is calculated according to the following Formula (52).

$$P_{HTE} = P_{HTE,Nominal} \cdot f_{SB} \cdot X_{SB} \tag{52}$$

f_{SB} has the value 1, because the whole electrolyzer stack is in standby.

The electrical power is calculated with the following formulas. The calculation varies on the case. Which formula is used in which case is stated in Table 10.

$$P_{el} = P_{HTE} + p_{air,comp} \cdot n_{Air,HTE} + p_{water,pump} \\ \cdot \left(n_{H2O,eva,HTE} + n_{TES,C,LT}\right) + n_{H2,feed} \cdot p_{heater,H2} \tag{53}$$

$$P_{el} = P_{HTE} + P_{HTE,part,SB} + p_{air,comp} \cdot n_{Air,HTE} + p_{water,pump} \\ \cdot n_{H2O,eva,HTE} + n_{H2,feed} \cdot p_{heater,H2} \tag{54}$$

$$P_{el} = P_{HTE} + p_{air,comp} \cdot n_{Air,HTE} + p_{water,pump} \cdot n_{H2O,eva,HTE} \\ + n_{H2,feed} \cdot p_{heater,H2} \tag{55}$$

Table 10 different electrical power calculations

case	Formula
1	(53)
2; 3; 4; 6; 7	(55)
5; 8	(54)

The detailed conditions, including the mass and mole flow calculations for the different cases, are given in the appendix B (Figure 35 to Figure 41).

Transient load and thermal storage integration analysis
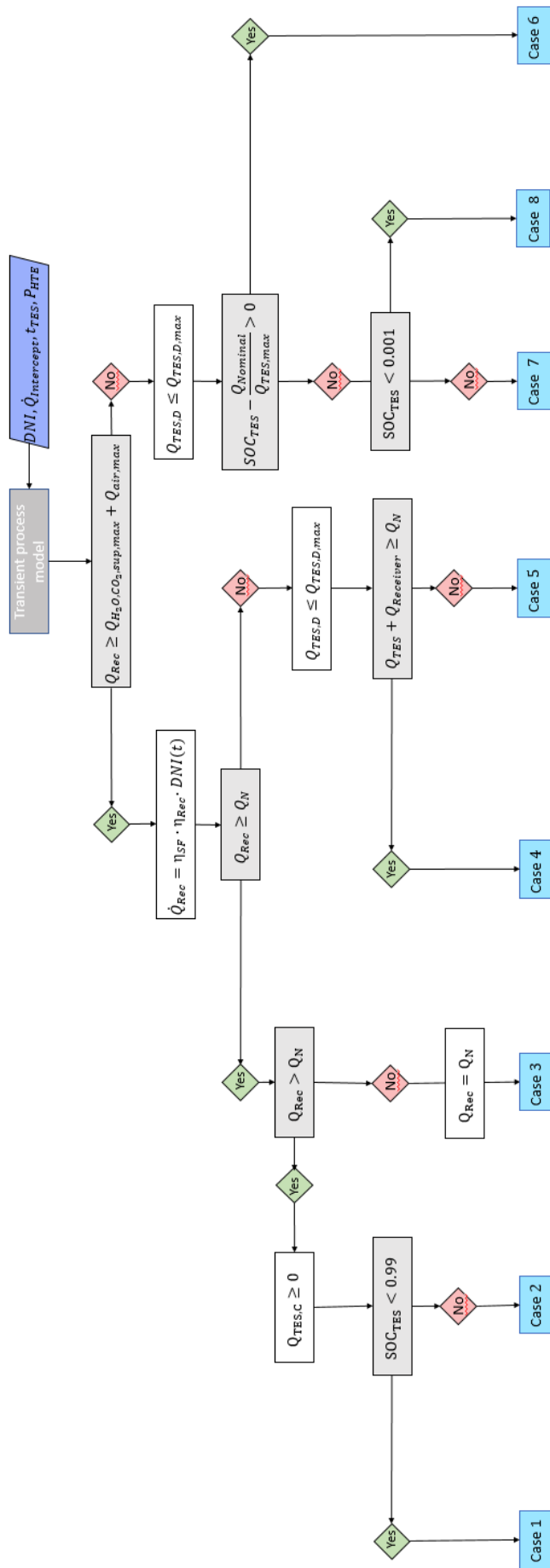
Figure 29 transient control algorithm

Transient load and thermal storage integration analysis

4.4   Results transient control algorithm

The different operating modes described in chapter 4.3 are integrated into a python model. The following values are stored in a csv file (co-electrolysis_hour_values) for each hour of the year.

- Receiver power
- Electrolyzer power (thermal)
- Electrical power
- Electrolyzer power (electric)
- Surplus energy
- SOC of the storage
- Charge power of the TES
- Discharge power of the TES
- Operation case

- Power of the air flow through the electrolyzer
- Power of the water evaporation flow through the electrolyzer
- Power of the water/carbon dioxide flow through the electrolyzer
- Mole flow syngas
- Mass flow syngas
- Mole flow air electrolyzer
- Mole flow water electrolyzer
- Mole flow water/carbon dioxide electrolyzer

In a different csv file (co-electrolysis_annual_values), the following annual values are saved.

- Nominal power electrolyzer
- Storage time TES
- Receiver power
- Electrical power
- Electrolyzer power
- Surplus power

- Charge power of the TES
- Discharge power of the TES
- Mole syngas
- Mass syngas

In Figure 30 different powers for one day (in this case the 21.03.) are plotted. The nominal power is the power that results from the Aspen simulation (26.241 kW). The TES has a storage capacity of 6 hours.

The day begins with no solar power and an empty storage. The electrolyzer is in standby mode, as shown in Figure 31. The power required for standby operation is supplied electrically. From 8 a.m. to 4 p.m. solar radiation (green line) hits the heliostat field. From 8 a.m. to 12 p.m. the storage is charged (light blue). From 12 p.m. the storage is full. Figure 32 shows the SOC of the storage. Beginning at 11 a.m., the receiver begins to provide more power than is needed for electrolysis and what can be stored. The surplus energy is shown by the purple line. From 4 p.m. on, the storage is discharged (dark blue line) so that the electrolyzer can be operated under nominal conditions till 10 p.m. During the last two hours of the day, the electrolyzer (red line) is in standby mode.

Transient load and thermal storage integration analysis
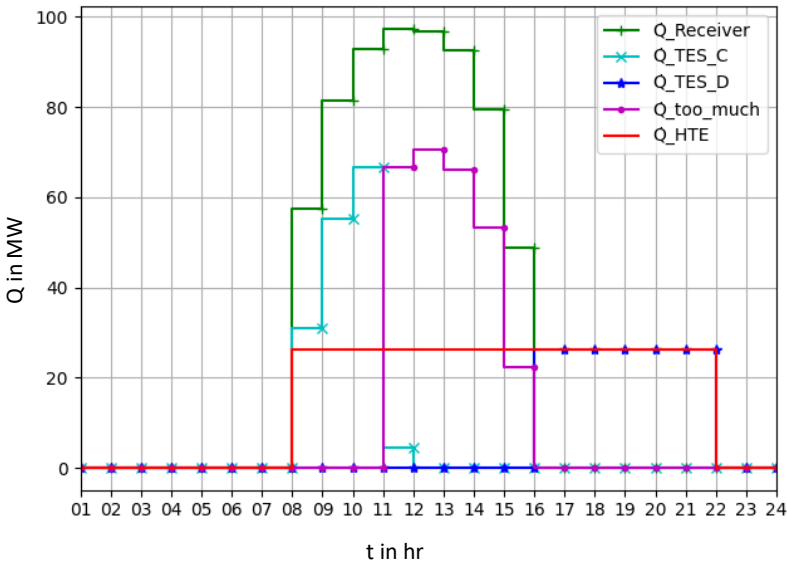
Figure 30 curve of different powers for the 21. of March for 26,241 MW nominal power and a thermal energy storage time of 6 hours
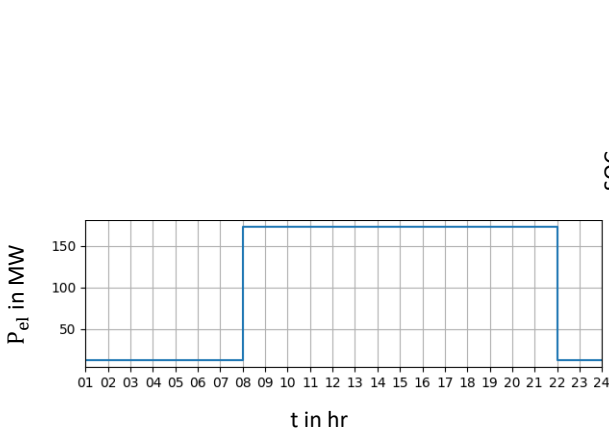
Figure 31 curve electrical power for the 21. of March for 26,241 MW nominal power and a thermal energy storage time of 6 hours
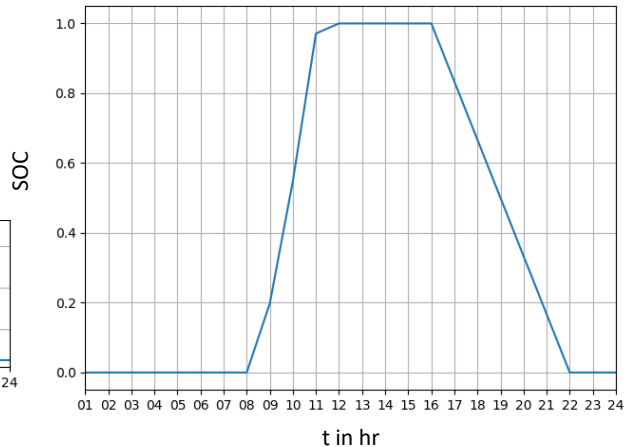
Figure 32 curve SOC thermal energy storage for the 21. of March for 26,241 MW nominal power and a thermal energy storage time of 6 hours

The size of the heliostat field, the size of the electrolyzer and the storage capacity are not well matched. The storage is already charged after 4 hours and too much energy is produced for 5 hours. Both the nominal power of the electrolyzer and the storage capacity can be modified. In the following, a parameter study is performed to better match the sizes. The nominal power is 25, 50 and 75 MW. The storage capacity is adjusted by varying the storage time. It ranges from 3 hours to 12 hours in 3-hour increments. Table 11 shows the annual values of various energies and the annual mass of syngas as a function of the nominal power and storage time.

Transient load and thermal storage integration analysis

Table 11 annual values parameter study

Configuration	$\dot{Q}_{Nominal}$ in MW	t_{TES} in hr	Q_{HTE} in GWh/a	E_{el} in GWh/a	E_{HTE} in GWh/a	Q_{too_much} in GWh/a	$Q_{TES,C}$ in GWh/a	$Q_{TES,D}$ in GWh/a	m_{syngas} in t/a
A	25	3	117	816	798	107.4	27	27	47,278
B	25	6	143	976	955	81.3	53	53	57,878
C	25	9	168	1125	1101	56.7	78	78	67,808
D	25	12	189	1259	1232	34.8	100	100	76,665
E	50	3	205	1451	1415	17.9	42	41	82,540
F	50	6	222	1560	1521	0.2	60	59	89,697
G	50	9	223	1561	1522	0.0	60	59	89,774
H	50	12	223	1561	1522	0.0	60	59	89,774
I	75	3	221	1639	1579	0.0	13	12	87,173
J	75	6	221	1639	1579	0.0	13	12	87,173
K	75	9	221	1639	1579	0.0	13	12	87,172
L	75	12	220	1639	1579	0.0	13	12	87,170

The receiver power for the year is 224,415 MWh. At a nominal load of 75 MW, almost the same amount of synthesis gas is produced regardless of the storage time. The electrical energy requirement is the same for all storage sizes. All the energy provided by the receiver can be used. Q_{too_much} is zero. However, the storage is never fully charged. Even at the shortest storage time of 3 hours, the maximum storage charge is less 60 %. Figure 33 shows the course of the soc for the days 21. to 24.03.
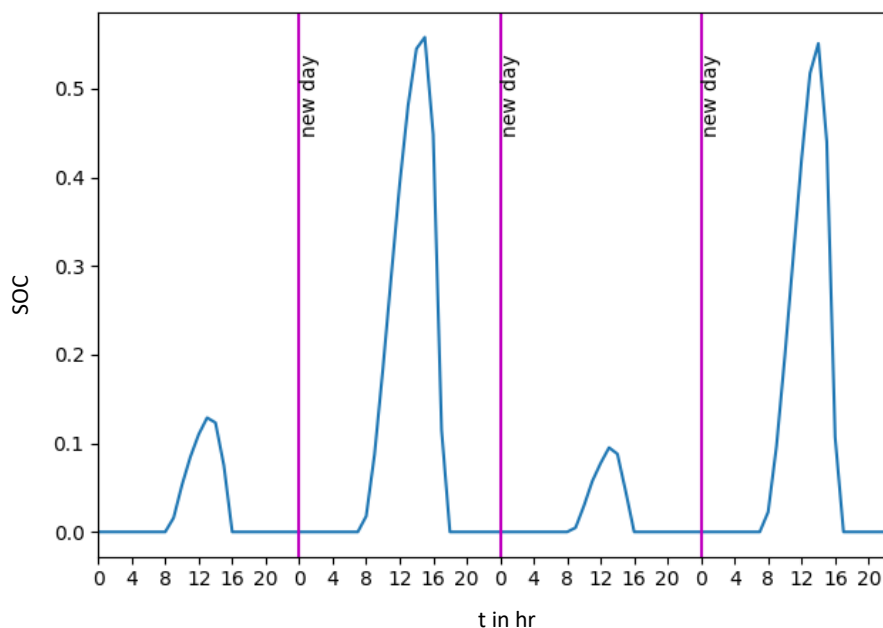
Figure 33 curve SOC: Q_Nominal=75 MW, t_TES=3 h, 21. to 24.03.

Transient load and thermal storage integration analysis

For the 25 and 50 MW nominal loads, the electrical energy requirement increases with increasing storage size and increasing nominal load. With a nominal capacity of 50 MW and a storage size of 9 and 12 hours, the entire receiver power can be used. These configurations produce the most syngas (89,774 t/a). A storage size of 12 hours has no advantage over 9 hours. All presented values are the same. With a storage capacity of 6 hours, the surplus energy is 200 MWh, with 3 hours almost 18 GWh. With 25 MW, the mass of produced syngas decreases with decreasing storage size, the surplus energy increases.

From a technical point of view, the preferred configuration is one with a rated load of 50 MW and a storage capacity of 6 or 9 hours because there is little or no surplus energy and most syngas is produced.

5 Techno-economic analysis

This chapter presents a brief techno-economic analysis. Investment and running costs are used to estimate the costs of the various configurations listed in the previous chapter 4.4. Investment costs are shown in Table 12.

Table 12 investment cost

investment costs	specific costs	units	source
solar tower	see Figure 42	€/m	(Reeken et al., 2016)
heliostat field	92.17	€/m²	(Rosenstiel, 2018)
high temperature electrolyzer	4000	€/kW	(International Energy Agency- IEA, 2019)
thermal energy storage	90	€/kWh	(International Renewable Energy Agency [IRENA], 2020)

The costs for the solar tower can be found in the appendix C. The sizes of the solar field and the solar tower are fixed. These costs are the same for each configuration (see Table 13).

Table 13 investment cost of solar tower and heliostat field

fixed investment costs	value	units	costs	units
solar tower	143	m	5,000,000	€
heliostat field	160,884.40	m²	14,828,715.10	€

The cost of the high temperature electrolyzer and thermal energy storage varies. Table 14 shows the cost of both components for each configuration. The storage capacity in kWh is required to calculate the storage cost. The cost of the electrolyzer is calculated using the power requirements of the electrolyzer.

Table 14 investment costs HTE and TES for all configurations

configuration	Q_TES in kWh	P_el in kW	costs HTE in €	costs TES in €
A	75,000	161,356	645,424,457	6,750,000
B	150,000	161,356	645,424,457	13,500,000
C	225,000	161,356	645,424,457	20,250,000
D	300,000	161,356	645,424,457	27,000,000
E	150,000	322,712	1,290,848,914	13,500,000
F	300,000	322,712	1,290,848,914	27,000,000
G	450,000	322,712	1,290,848,914	40,500,000
H	600,000	322,712	1,290,848,914	54,000,000
I	225,000	484,068	1,936,273,371	20,250,000
J	450,000	484,068	1,936,273,371	40,500,000
K	675,000	484,068	1,936,273,371	60,750,000
L	900,000	484,068	1,936,273,371	81,000,000

Techno-economic analysis

With an assumed lifetime of 20 years and an interest rate of 6 %, the following annual costs result from formula 4 (see Table 15). A is the annual cost, C is the investment cost.

$$A = C \cdot \frac{(1+i)^n \cdot i}{(1+i)^n - 1}$$ (56)

Table 15 total and annual investment costs

configuration	total investment costs in €	annual investment costs in €
A	672,003,172	58,588,299
B	678,753,172	59,176,795
C	685,503,172	59,765,290
D	692,253,172	60,353,786
E	1,324,177,629	115,447,840
F	1,337,677,629	116,624,831
G	1,351,177,629	117,801,823
H	1,364,677,629	118,978,814
I	1,976,352,086	172,307,381
J	1,996,602,086	174,072,868
K	2,016,852,086	175,838,356
L	2,037,102,086	177,603,843

The ongoing cost of electricity is assumed to be 5 cent per kWh (Fraunhofer ISE, 2021). Table 16 shows the annual electricity costs for all configurations. They can be calculated depending on the annual electricity demand.

Table 16 annual electricity costs

configuration	E_el in kWh	electricity costs in T€
A	815,586,597	40,779,330
B	975,576,270	48,778,814
C	1,125,467,805	56,273,390
D	1,259,267,458	62,963,373
E	1,451,441,098	72,572,055
F	1,560,097,423	78,004,871
G	1,561,327,152	78,066,358
H	1,561,327,152	78,066,358
I	1,638,752,097	81,937,605
J	1,638,752,097	81,937,605
K	1,638,752,646	81,937,632
L	1,638,663,685	81,933,184

To calculate the levelized costs of syngas (LCOS) Formula (57) is used.

$$LCOS = \frac{investment\ costs + running\ costs}{mass\ syngas\ per\ year}$$ (57)

Techno-economic analysis

Table 17 levelized costs of syngas for all configurations

configuration	m_syngas in kg/a	LCOS in €/kgsyngas
A	47,278,314	864
B	57,877,718	844
C	67,807,611	831
D	76,665,211	822
E	82,540,024	881
F	89,696,860	871
G	89,773,866	871
H	89,773,866	871
I	87,172,913	942
J	87,172,913	942
K	87,172,405	942
L	87,169,990	942

Configuration D has the lowest LCOS. This is the configuration with an electrolyzer with a nominal load of 25 MW and a storage time of 12 hours. With this configuration, the cost per kilogram of syngas is 822 euros.
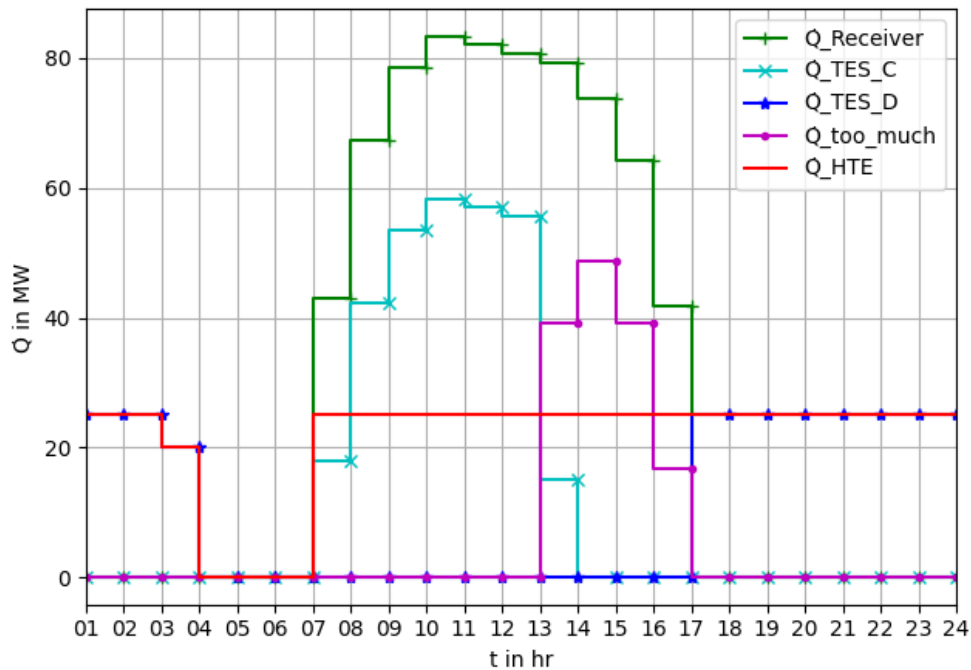

Figure 34 curves of different powers for the 21. of March for 25 MW nominal power and a thermal energy storage time of 12 hours

Figure 34 shows configuration D. The electrolyzer can run at full load for 19 hours. The storage is loaded for 7 hours and unloaded for 10 hours. 76,665 tons of syngas are produced per year and 1259 GWh of electricity are required.

6   Summary

In this thesis, a co-electrolysis process using concentrated solar energy was technically and economically analyzed. Co-electrolysis can be used to produce syngas, a mixture of hydrogen and carbon monoxide. To introduce the topic, the basics of high-temperature- and co-electrolysis as well as concentrated solar energy were described. Co-electrolysis is a high-temperature electrolysis process in which the required thermal energy can be provided by concentrated solar energy. During the electrolysis, water and carbon dioxide are reduced to form hydrogen and carbon monoxide. At the same time, an equilibrium reaction, the RWGS reaction, takes place. To obtain the thermal and electrical energy requirements a simulation was done in aspen. Due to the complexity and lack of experimental data, simulations of co-electrolysis have different approaches. The approach of 5 publications was compared. Key variables compared were temperature, RU, inlet and outlet mole fractions, and molar ratios. The temperature range considered is greater than 150 °C. The RU of water varies between 0.2 and 0.98, the RU of carbon dioxide varies between 0.05 and 0.73. The inlet mole fractions are also different. One publication has only water and carbon dioxide as input. Another one, recycles more than 70 % of hydrogen and carbon monoxide. This leads to different results in the publications. The product stream of one publication still contains more than 75 % molar fraction of water and carbon dioxide. Another publication has more than 90 % molar fraction of hydrogen and carbon dioxide. Thus, the published molar ratios of hydrogen to carbon dioxide vary. The molar ratio ranges from just under 1 to 2.

Based on the literature, four electrolysis models were developed. Model 1 uses a stoichiometric reactor and separator to simulate electrolysis. Models 2 and 3 have two additional equilibrium reactors to include the RWGS. In Model 2, the first equilibrium reactor is operated at a lower temperature than the stoichiometric reactor. Model 3 operates all components at the same temperature. Model 4 consists of the stoichiometric reactor, the separator, and an equilibrium reactor after the separator.

The results of the simulations were compared with literature data. Between the simulated and published outlet mass flows there are deviations between -15 % and +16 %. Negative deviations indicate that the simulated mass flow is lower than the published values. Mainly water and carbon monoxide streams have negative deviations. Models 2, 3 and 4 give almost identical results for the outlet mass flows. When comparing the electrical energy requirements, the difficulty is that aspen only calculates the chemical energy requirement, while the electrical (system) energy requirement is usually published in the literature. One literature source also published the chemical energy requirement. When comparing the chemical energy requirements of the simulation and the publication, electrolyzer model 3

Summary

has the highest agreement with more than 99.3 %. Based on this comparison, Model 3 was selected as having the best correlation with literature data. Model 3 was validated with experimental data. Comparison with experimental data showed deviations of less than 5 %. This electrolyzer model is embedded in aspen.

The electrolyzer temperature is 820 °C, the electrolyzer pressure is one bar. The RU for water and carbon dioxide is 70 %. The inlet molar fraction of water is 56.5 %, that of carbon dioxide is 33.5 %, and that of hydrogen is 10 %. This results in an outlet molar ratio of 2:1 (hydrogen to carbon monoxide). The specific thermal energy demand is 46.9 kWh per kmol of syngas and the specific electric energy demand is 300.7 kWh per kmol of syngas. With these values, an existing transient Python model for steam electrolysis was adapted to co-electrolysis.

To ensure continuous operation, a thermal energy storage was implemented in the process. For relevant components mass and energy balances were calculated and implemented in the code. Depending on the DNI and the SOC of the storage, the electrolyzer is provided with different power and different mass flows flow through the receiver. Through a parameter study, the heliostat field, the electrolyzer size and the storage capacity were adjusted. The heliostat field has a fixed area of 160,884.4 m². The nominal power of the electrolyzer was varied between 25, 50 and 75 MW, the storage capacity between 3, 6, 9 and 12 hours. From a technical point of view, a configuration with a nominal power of 50 MW and a storage capacity of 6 or 9 hours was recommended. This is because most of the syngas is produced (89,700 tons per year) and there is little or no excess energy. Approximately 1560 GWh per year are needed for these configurations.

Finally, a brief economic analysis was performed. Prices for the solar tower, the heliostat field, the high-temperature electrolyzer, the thermal energy storage, and the electricity demand were determined. The levelized cost of syngas was then calculated for all configurations. The 25 MW nominal power configuration with a 12-hour storage period has the lowest LCOS.

The parameter study could be further developed to determine the technically optimal configuration of the co-electrolysis process. Not only the nominal power of the electrolyzer and the storage capacity should be considered, but also other relevant parameters such as efficiency, lifetime of components and operating conditions. A detailed sensitivity analysis could provide insight into how changes in the parameters affect the overall performance. The economic side of the co-electrolysis process should be further investigated. Here, subsidies and carbon dioxide prices play a decisive role. How do government subsidies or tax

Summary

incentives affect the economics? Which cost factors are particularly relevant? To validate the simulation results, further experiments should be performed. This could be done both in the laboratory and on an industrial scale. Practical tests can help to verify the accuracy of the models and increase the reliability of the simulations.

7   References

Ausfelder, F., & Wagemann, K. (2020). Power-to-fuels: E-fuels as an Important Option for a Climate-Friendly Mobility of the Future. *Chemie Ingenieur Technik*, *92*(1-2), 21–30. https://doi.org/10.1002/cite.201900180

Bachmann, M., Völker, S., Kleinekorte, J., & Bardow, A. (2023). *Syngas from what? Comparative Life-Cycle Assessment for Syngas Production from Biomass, CO 2, and Steel Mill Off-Gases*. Universitätsbibliothek der RWTH Aachen. https://doi.org/10.18154/RWTH-2023-04890

Dueñas, D. M. A., Riedel, M., Riegraf, M., Costa, R., & Friedrich, K. A [Kaspar Andreas] (2020). High Temperature Co-electrolysis for Power-to-X. *Chemie Ingenieur Technik*, *92*(1-2), 45–52. https://doi.org/10.1002/cite.201900119

Fraunhofer ISE. (2021). *Levelized Cost of Electricity: Renewables Clearly Superior to Conventional Power Plants Due to Rising CO2 Prices*. https://www.ise.fraunhofer.de/en/press-media/press-releases/2021/levelized-cost-of-electricity-renewables-clearly-superior-to-conventional-power-plants-due-to-rising-co2-prices.html

Fu, Q., Mabilat, C., Zahid, M., Brisse, A., & Gautier, L. (2010). Syngas production via high-temperature steam/CO2 co-electrolysis: an economic assessment. *Energy & Environmental Science*, *3*(10), 1382. https://doi.org/10.1039/c0ee00092b

Graves, C., Ebbesen, S. D., & Mogensen, M. (2011). Co-electrolysis of CO2 and H2O in solid oxide cells: Performance and durability. *Solid State Ionics*, *192*(1), 398–403. https://doi.org/10.1016/j.ssi.2010.06.014

Hawkes, G. (2007). *3D CFD Model of High Temperature H2O/CO2 Co-electrolysis.*

Herz, G., Reichelt, E., & Jahn, M. (2018). Techno-economic analysis of a co-electrolysis-based synthesis process for the production of hydrocarbons. *Applied Energy*, *215*, 309–320. https://doi.org/10.1016/j.apenergy.2018.02.007

International Energy Agency- IEA. (2019). *The Future of Hydrogen: Seizing today's opportunities*. https://iea.blob.core.windows.net/assets/9e3a3493-b9a6-4b7d-b499-7ca48e357561/The_Future_of_Hydrogen.pdf

International Renewable Energy Agency. (2020). *Innovation outlook: Thermal energy storage*. https://www.irena.org/-/media/Files/IRENA/Agency/Publication/2020/Nov/IRENA_Innovation_Outlook_TES_2020.pdf?rev=6950b7b9792344b5ab28d58e18209926

Khesa, N., & Mulopo, J. (2021). Performance evaluation, Optimization and exergy analysis of a high temperature co-electrolysis power to gas process using Aspen Plus®-a model

References

based study. *Energy Science & Engineering*, *9*(11), 1950–1960. https://doi.org/10.1002/ese3.947

Langie, K. M. G., Tak, K., Kim, C., Lee, H. W., Park, K., Kim, D., Jung, W., Lee, C. W., Oh, H.-S., Lee, D. K., Koh, J. H., Min, B. K., Da Won, H., & Lee, U. (2022). Toward economical application of carbon capture and utilization technology with near-zero carbon emission. *Nature Communications*, *13*(1), 7482. https://doi.org/10.1038/s41467-022-35239-9

Larsen, H., & Sønderberg Petersen, L. *Energy technologies for post Kyoto targets in the medium term: Proceedings : Risø International Energy Conference : Risø National Laboratory 19-21 May 2003. Risø-R: 1405 (EN)*. Risø DTU - National Laboratory for Sustainable Energy; available from: Risø National Laboratory, Information Service Department.

Lovegrove, K. (2021). *Concentrating solar power technology: Principles, developments, and applications* (Second edition). *Woodhead Publishing Series in Energy*. Elsevier; Woodhead Publishing.

O'Brien, J. E., McKellar, M. G., Harvego, E. A., & Stoots, C. M [C. M.] (2010). High-temperature electrolysis for large-scale hydrogen and syngas production from nuclear energy – summary of system simulation and economic analyses. *International Journal of Hydrogen Energy*, *35*(10), 4808–4819. https://doi.org/10.1016/j.ijhydene.2009.09.009

Peters, R., Wegener, N., Samsun, R. C., Schorn, F., Riese, J., Grünewald, M., & Stolten, D. (2022). A Techno-Economic Assessment of Fischer–Tropsch Fuels Based on Syngas from Co-Electrolysis. *Processes*, *10*(4), 699. https://doi.org/10.3390/pr10040699

Petipas, F., Brisse, A., & Bouallou, C. (2013). Model-based behaviour of a high temperature electrolyser system operated at various loads. *Journal of Power Sources*, 584–595.

Redissi, Y., & Bouallou, C. (2013). Valorization of Carbon Dioxide by Co-Electrolysis of CO2/H2O at High Temperature for Syngas Production. *Energy Procedia*, *37*, 6667–6678. https://doi.org/10.1016/j.egypro.2013.06.599

Reeken, F. von, Weinrebe, G., Keck, T., & Balz, M. (2016). Heliostat cost optimization study. In *AIP Conference Proceedings* (p. 160018). Author(s). https://doi.org/10.1063/1.4949259

Roeder, T. (2023). *CO-Electrolysis.* DLR.

Rosenstiel, A. (2018). Techno-economic study of a concentrated solar thermal plant with sulphur as thermochemical energy storage for baseload power generation and sulphuric acid recycling.

References

Schmidt, T. (2022). *Wasserstofftechnik*. Carl Hanser Verlag GmbH & Co. KG.
https://doi.org/10.3139/9783446473539

Stoots, C. M [Carl M.], O'Brien, J. E., Herring, J. S., & Hartvigsen, J. J. (2009). Syngas
Production via High-Temperature Coelectrolysis of Steam and Carbon Dioxide.
Journal of Fuel Cell Science and Technology, *6*(1), Article 011014.
https://doi.org/10.1115/1.2971061

Tandl, M. (2023). *Co-SOEC vs SOEC+rWGS*.

Tomberg, M., Heddrich, M. P., Ansar, S. A., & Friedrich, K. A [K. Andreas] (2023). Operation
strategies for a flexible megawatt scale electrolysis system for synthesis gas and
hydrogen production with direct air capture of carbon dioxide. *Sustainable Energy &
Fuels*, *7*(2), 471–484. https://doi.org/10.1039/d2se01473d

Töpler, J., & Lehmann, J. (Eds.). (2017). *Wasserstoff und Brennstoffzelle: Technologien und
Marktperspektiven* (2., aktualisierte und erweiterte Auflage). Springer Vieweg.
https://doi.org/10.1007/978-3-662-53360-4

8 Appendix

A. Molar fractions literature

Table 18 inlet molar fractions literature

inlet molar fractions	Tomberg	Dueñas et al., 2020	Khesa & Mulopo, 2021	Redissi & Bouallou, 2013	Tandl, 2023
H_2O	0.565	0.654	0.5	0.45	0.168
CO_2	0.335	0.296	0.5	0.45	0.091
H_2	0.1	0.033		0.1	0.490
CO		0.017			0.244
CH_4					0.007

Table 19 outlet molar fractions literature

outlet molar fraction	Tomberg	Dueñas et al., 2020	Khesa & Mulopo, 2021	Redissi & Bouallou, 2013	Tandl, 2023
H_2O	0.1695	0.5240	0.2807	0.2333	0.0464
CO_2	0.1005	0.2320	0.2791	0.2010	0.0238
H_2	0.4955	0.1630	0.2175	0.3167	0.6110
CO	0.2345	0.0810	0.2227	0.2490	0.3119
CH_4					0.0070

B. Mass and molar flow calculations control algorithm

```
m_TES_C_LT = m_H2O_eva_receiver - m_H2O_eva_HTE_nominal
m_TES_C_HT = m_H2OCO2_sup_receiver - m_H2OCO2_sup_HTE_nominal
m_H2O_eva_HTE = m_H2O_eva_HTE_nominal
m_H2OCO2_sup_HTE = m_H2OCO2_sup_HTE_nominal
m_Air_HTE = m_Air_HTE_nominal
m_syngas = P_HTE / p_syngas_mass
n_TES_C_LT = n_H2O_eva_receiver - n_H2O_eva_HTE_nominal
n_TES_C_HT = n_H2OCO2_sup_receiver - n_H2OCO2_sup_HTE_nominal
n_H2O_eva_HTE = n_H2O_eva_HTE_nominal
n_H2OCO2_sup_HTE = n_H2OCO2_sup_HTE_nominal
n_Air_HTE = n_Air_HTE_nominal
n_syngas = P_HTE / p_snygas
```

Figure 35 mass and mole flow equations control algorithm case 1

Appendix

```
m_H2O_eva_HTE = m_H2O_eva_HTE_nominal
m_H2OCO2_sup_HTE = m_H2OCO2_sup_HTE_nominal
m_Air_HTE = m_Air_HTE_nominal
m_syngas = P_HTE / p_syngas_mass
n_H2O_eva_HTE = n_H2O_eva_HTE_nominal
n_H2OCO2_sup_HTE = n_H2OCO2_sup_HTE_nominal
n_Air_HTE = n_Air_HTE_nominal
n_syngas = P_HTE / p_snygas
```

Figure 36 mass and mole flow equations control algorithm case 2 and 3

```
m_TES_D_LT = m_H2O_eva_HTE_nominal - m_H2O_eva_receiver
m_H2O_eva_HTE = m_H2O_eva_HTE_nominal
m_H2OCO2_sup_HTE = m_H2OCO2_sup_HTE_nominal
m_Air_HTE = m_Air_HTE_nominal
m_syngas = P_HTE / p_syngas_mass
n_TES_D_LT = n_H2O_eva_HTE_nominal - n_H2O_eva_receiver
n_H2O_eva_HTE = n_H2O_eva_HTE_nominal
n_H2OCO2_sup_HTE = n_H2OCO2_sup_HTE_nominal
n_Air_HTE = n_Air_HTE_nominal
n_syngas = P_HTE / p_snygas
```

Figure 37 mass and mole flow equations control algorithm case 4

```
Q_Air_HTE = 0.06383 * Q_HTE
Q_H2OCO2_sup_HTE = 0.17484 * Q_HTE
Q_H2O_eva_HTE = 0.76133 * Q_HTE
m_H2O_eva_HTE = (Q_H2O_eva_HTE * 3600000) / delta_h_H2O_eva
m_TES_D_LT = m_H2O_eva_HTE - m_H2O_eva_receiver
m_H2OCO2_sup_HTE = m_H2OCO2_sup_HTE_nominal
m_Air_HTE = m_Air_HTE_nominal
m_syngas = (P_HTE - P_HTE_part_SB) / p_syngas_mass #kg/hr
n_H2O_eva_HTE = (Q_H2O_eva_HTE * 3600000) / delta_hm_H2O_eva
n_TES_D_LT = n_H2O_eva_HTE - n_H2O_eva_receiver
n_H2OCO2_sup_HTE = n_H2OCO2_sup_HTE_nominal
n_Air_HTE = n_Air_HTE_nominal
n_syngas = (P_HTE - P_HTE_part_SB) / p_snygas #kmol/hr
```

Figure 38 mass and mole flow equations control algorithm case 5

Appendix

```
m_TES_D_LT = m_H2O_eva_HTE_nominal
m_TES_D_HT = m_H2OCO2_sup_HTE_nominal
m_H2O_eva_HTE = m_H2O_eva_HTE_nominal
m_H2OCO2_sup_HTE = m_H2OCO2_sup_HTE_nominal
m_Air_HTE = m_Air_HTE_nominal
m_syngas = P_HTE / p_syngas_mass
n_TES_D_LT = n_H2O_eva_HTE_nominal
n_TES_D_HT = n_H2OCO2_sup_HTE_nominal
n_H2O_eva_HTE = n_H2O_eva_HTE_nominal
n_H2OCO2_sup_HTE = n_H2OCO2_sup_HTE_nominal
n_Air_HTE = n_Air_HTE_nominal
n_syngas = P_HTE / p_snygas
```

Figure 39 mass and mole flow equations control algorithm case 6

```
m_H2O_eva_HTE = 0
m_H2OCO2_sup_HTE = 0
m_Air_HTE = 0
m_syngas = 0
n_H2O_eva_HTE = 0
n_H2OCO2_sup_HTE = 0
n_Air_HTE = 0
n_syngas = 0
```

Figure 40 mass and mole flow equations control algorithm case 7

```
Q_Air_HTE = 0.06383 * Q_HTE
Q_H2OCO2_sup_HTE = 0.17484 * Q_HTE
Q_H2O_eva_HTE = 0.76133 * Q_HTE
m_H2O_eva_HTE = (Q_H2O_eva_HTE * 3600000)/ delta_h_H2O_eva
m_TES_D_LT = m_H2O_eva_HTE - m_H2O_eva_receiver
m_H2OCO2_sup_HTE = (Q_H2OCO2_sup_HTE * 3600000) / delta_h_H2OCO2_sup
m_Air_HTE = (Q_Air_HTE * 3600000) / delta_h_Air
m_syngas = (P_HTE - P_HTE_part_SB) / p_syngas_mass #kg/hr
n_H2O_eva_HTE = (Q_H2O_eva_HTE * 3600000) / delta_hm_H2O_eva
n_TES_D_LT = n_H2O_eva_HTE - n_H2O_eva_receiver
n_H2OCO2_sup_HTE = (Q_H2OCO2_sup_HTE * 3600000) / delta_hm_H2OCO2_sup
n_Air_HTE = (Q_Air_HTE * 3600000) / delta_hm_Air
n_syngas = (P_HTE - P_HTE_part_SB) / p_snygas #kmol/hr
```

Figure 41 mass and mole flow equations control algorithm case 8
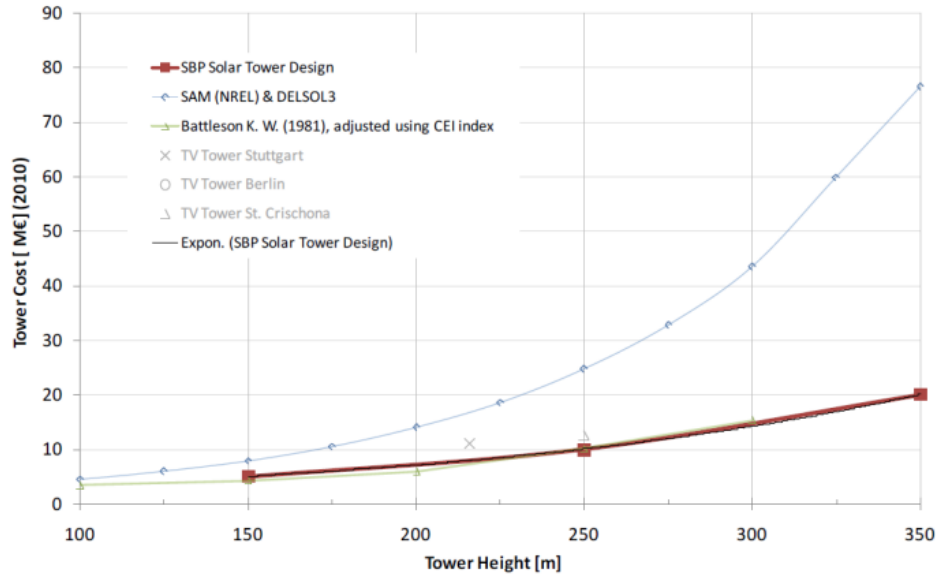
Appendix

C. Solar tower costs

Figure 42 tower cost depending on the hight of the solar tower, costs are shown in red (Reeken et al., 2016)

Appendix

D. Digital appendix

Main folder:

- **Pdf version of this thesis**
  Masterarbeit_Lindermeir_Hannah_379618.pdf

References

- **Fraunhofer ISE. (2021). Levelized Cost of Electricity: Renewables Clearly Superior to Conventional Power Plants Due to Rising CO2 Prices.**
  Fraunhofer_ISE_(2021)_Levelized_cost_of_electricity.pdf
- **International Energy Agency- IEA. (2019). The Future of Hydrogen: Seizing today's opportunities**.
  International_Energy_Agency_IEA_(2019)_The_Future_of_Hydrogen.pdf
- **International Renewable Energy Agency. (2020). Innovation outlook: Thermal energy storage.**
  International_Renewable_Energy_Agency_(2020)_Innovation_Outlook.pdf
- **Roeder, T. (2023). CO-Electrolysis.**
  Roeder,Timo_(2023)_CO-Electrolysis.pdf
- **Rosenstiel, A. (2018). Techno-economic study of a concentrated solar thermal plant with sulphur as thermochemical energy storage for baseload power generation and sulphuric acid recycling.**
  Rosenstiel,Andreas_(2018)_Techno-economic_study_of_a_concentrated_solar_thermal_plant.pdf
- **Tandl, M. (2023). Co-SOEC vs SOEC+rWGS.**
  Tandl_(2023)_Co-SOEC_vs_SOEC+RWGS.pdf

Source code

- **Python source code co-electrolysis**
  Coelectrolysis.py
- **DNI data Ouarzazate**
  1_Ouarzazate-hour.csv
- **Results co-electrolysis annual values**
  co-electrolysis_annual_values.csv
- **Results co-electrolysis hour values**
  co-electrolysis_hour_values.csv
- **Field efficiency Ouarzazate**
  df_eff_100MWth_1_Ouarzazate.csv

Erklärung

Ich versichere, dass ich diese Masterarbeit selbstständig angefertigt, nicht anderweitig für Prüfungszwecke vorgelegt, alle benutzten Quellen und Hilfsmittel angegeben, sowie wörtliche und sinngemäße Zitate gekennzeichnet habe.

Kempten, den..

Ermächtigung

Hiermit ermächtige ich die Hochschule Kempten zur Veröffentlichung der Kurzzusammenfassung (Abstract) meiner Arbeit, z. Bsp. auf gedruckten Medien oder auf einer Internetseite.

Kempten, den ....